Magnetic neutron scattering from two-dimensional lattice electrons: The case of La$_{2-x}$Sr$_x$CuO$_4$

Pierre Bénard, Liang Chen, and A.-M. S. Tremblay

*Département de Physique and Centre de Recherche en Physique du Solide,
Université de Sherbrooke, Sherbrooke, Québec, Canada J1K 2R1*
(Received 14 December 1992)

It is found that the one-band Hubbard model, in the weak- to intermediate-coupling regime, can account qualitatively for magnetic-neutron-scattering experiments in the paramagnetic phase of La$_{2-x}$Sr$_x$CuO$_4$ when second-neighbor hopping is included. However, the peak *positions*, which in two dimensions are determined mostly by the band structure, cannot agree quantitatively with the experimental results when concentration-independent band parameters are used. More importantly, while the energy scale of roughly 150 K seen in the experiments can come from second-neighbor hopping, it arises most naturally if one is very close to a magnetic instability. The proximity to a magnetic instability can be checked experimentally by measuring the relative size of the lattice equivalent of $2k_F$ anomalies that appear closer to the origin in wave-vector space. Such lattice-$2k_F$ anomalies would allow magnetic neutron scattering to become a spectroscopic tool for the two-dimensional Fermi surface. Finally, exact results are also given for the imaginary part of the Lindhard function on the square lattice.

I. INTRODUCTION

High-energy experimental probes of high-temperature superconductors, such as x-ray-absorption spectroscopy (XAS), electron-energy-loss spectroscopy (EELS), and photoemission spectroscopy all seem to be consistent with an effective one-band Hubbard Hamiltonian[1] which in the electron picture takes the form

$$H = \left[-t \sum_{\langle i,j \rangle} c^{\dagger}_{\sigma i} c_{\sigma j} - t' \sum_{\langle\langle i,j \rangle\rangle} c^{\dagger}_{\sigma i} c_{\sigma j} + \text{H.c.} \right] + U \sum_i n_{i\uparrow} n_{i\downarrow} . \quad (1)$$

Various estimates of the parameters, based both on band-structure calculations[2] and comparisons of experiments with cluster calculations,[1] usually yield sizable values for the next-nearest-neighbor hopping t', as well as strong on-site repulsion U: For La$_{2-x}$Sr$_x$CuO$_4$, $t=0.43$ eV, $t'=-0.16t$, and $U=9.5t$ are typical values.

It is still an open question whether this Hamiltonian correctly describes the low-energy physics of high-temperature superconductors, even normal-state properties, let alone superconductivity. However, it is certainly a more generic model than the $t'=0$ model where Van Hove singularity and nesting all coincide at exactly half filling. More importantly, from a perturbative point of view the $t' \neq 0$ model is at least a better starting point for low-energy properties than the usual $t'=0$ model. Indeed, the sign and doping dependence of the Hall coefficient, thermopower, as well as the qualitative dependence of the uniform magnetic susceptibility on temperature and doping are all correct when t' differs from zero, contrary to the $t'=0$ case where it is hoped that all these properties will acquire the correct behavior in the strong-coupling limit. There have been several theoretical studies of this model using slave-boson approaches.[3−5]

For quantitative comparisons between low-energy experiments and theory, we believe that the magnetic structure factor is an ideal quantity to study. Indeed, it can both be computed reliably and measured in detail as a function of wave vector and frequency. On the experimental side, there have been several detailed neutron-scattering measurements of this quantity in the new superconductors.[6−11] Nuclear magnetic resonance[12−14] (NMR) is also a zero-frequency probe of the magnetic fluctuations but we concentrate on the neutron-scattering results whose interpretation does not require extra parameters such as hyperfine couplings. On the theoretical side, Monte Carlo calculations have shown that up to the intermediate-coupling regime, standard generalized random-phase approximation (GRPA) calculations give extremely accurate results for the magnetic structure factor as long as one accounts for a renormalization of the interaction U which comes from maximally crossed diagrams.[15,16] Physically this Kanamori-Brueckner renormalization comes about because of two-body correlations which reduce the amplitude of the two-body wave function for two antiparallel spins on the same site. This means that even in the intermediate-coupling regime, which is generally believed to be relevant for high-temperature superconductors,[12,13,17−23] spin-spin correlations can be accurately calculated from the weak-coupling approach with a renormalized value of U. The renormalized value of U can be estimated as shown in Ref. 15. Too close to half filling, however, large critical fluctuations in two dimensions should lead to the failure of the above approach.

Since our calculation should be valid up to the intermediate-coupling regime, disagreement with experiment would suggest either that it is fundamental to include the fluctuations responsible for the absence of finite-temperature long-range order in two dimensions,[14,23,24] or that only the very strong-coupling regime is relevant.[25−28] The only possibility left outside of these

<u>47</u>   15 217

two is that the one-band Hubbard model does not provide an accurate description of high-temperature superconductors. The calculations will be confined to the metallic phase.

In $YBa_2Cu_3O_{7-x}$, where numerous experiments have been performed,[9-11,29] the theoretical analysis is complicated by the presence of chains which lead to a more complex band structure.[2] Furthermore, the effective one-band Hamiltonian for this material has $|t'| \approx 0.5t$, leading to a 45° rotation of the Fermi surface and to a different class of problems. We thus concentrate instead on the simpler $La_{2-x}Sr_xCuO_4$ compound with $|t'| < 0.5t$. The main features of the experiment which we try to explain are illustrated in Fig. 1, taken from Ref. 6. One can see clear incommensurate peaks whose intensity, relative to the intensity at (π,π), has decreased by a factor of about 2 when the energy transfer is around 15 meV. The peaks are located at $\{(\pm\pi \mp \delta\pi, \pm\pi), (\pm\pi, \pm\pi \mp \delta\pi)\}$, in units where the lattice spacing is unity. (In the scan of Fig. 1, only two peaks show up.) The questions are the following: (a) Why do the peaks appear further away from (π,π) than one would expect from the simplest $t'=0$ model? (b) Where does the small energy scale of 15 meV come from? In Refs. 30 and 31 the position of the peaks was explained by a three-band model fit to the true band structure, while the energy dependence was ascribed purely to self-energy effects which arise in the marginal Fermi-liquid (MFL) approach.[30-32]

In Sec. II, we discuss the noninteracting limit of the model to remind the reader that from a perturbative point of view, the $t'\neq 0$ is a better starting point for the description of high-temperature superconductors than the conventional nearest-neighbor model. We also explain that, in two dimensions, it is mostly the shape of the Fermi surface in the noninteracting limit which determines the location of the intensity maxima in low-energy neutron scattering. This is why in Sec. III we examine the structure factor of the system with no interaction both in the case of vanishing $(t'=0)$, and in the case of finite next-nearest-neighbor hopping t'. We call the maxima in the noninteracting limit, lattice-$2k_F$ anomalies.
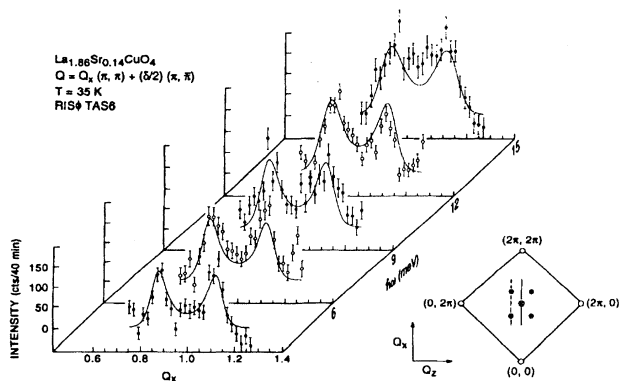

FIG. 1. Wave-vector scan of the magnetic structure factor for various energies, as measured experimentally (from Mason et al., Ref. 6).

The largest of these is determined by what we call pseudonesting. The various energy scales appearing in this noninteracting limit are discussed and argued to be generally too large, except for special values of t' and filling. In Sec. IV, we examine the effects of the Hubbard interaction, paying special attention to the spin-density-wave paramagnon that appears because of the on-site Coulomb repulsion. The proximity to zero frequency of an overdamped collective mode which softens at the incommensurate transition may give the small energy scale found in experiment. If this explanation is incorrect, as suggested, for example, in the MFL approach,[30] neutron-scattering experiments should clearly show concomitant incommensurate features nearer to the origin in reciprocal space.[23] Finally, in the last section, we make detailed comparisons with experimental data and suggest further key experiments. The first appendix contains the exact result for the imaginary part of the Lindhard function on the square lattice in the case of nearest-neighbor hopping, while the two other appendices contain various other analytical results in the case of finite t'.

II. BAND-STRUCTURE EFFECTS AND PSEUDONESTING

In the noninteracting limit, with unit lattice spacing, the dispersion relation is given by

$$\varepsilon(k) = -2t[\cos(k_x) + \cos(k_y)]$$
$$-2t'[\cos(k_x + k_y) + \cos(k_x - k_y)]$$
$$= -2t[\cos(k_x) + \cos(k_y)] - 4t' \cos(k_x)\cos(k_y).$$

(2)

The corresponding Fermi surface is plotted in Fig. 2 for various fillings. We restrict ourselves to $|t'| \leq |-0.5t|$ appropriate for $La_{2-x}Sr_xCuO_4$. In the opposite limit the Fermi surface topology changes completely and results are very different. In Fig. 2, the second-neighbor hopping parameter is chosen as $t'=-0.16t$, a value for $La_{2-x}Sr_xCuO_4$ which is consistent with local-density approximation (LDA) calculations and comparisons with x-ray-absorption experiments.[1] At half filling, orbits are open whereas sufficiently far from half filling, the orbits close again. In the intermediate case, the Fermi energy, equal to $4t'$, lies at a Van Hove singularity, as illustrated in the density-of-states plot of Fig. 3(a). That single-spin density of states is given by

$$N(\omega) = \frac{1}{2\pi^2[t^2 - t'\omega]^{1/2}} K\left[\left[\frac{16t^2 - (\omega + 4t')^2}{16(t^2 - t'\omega)}\right]^{1/2}\right],$$

(3)

where $K(x)$ is the complete elliptic integral of the first kind. The band extends in the range $-4t - 4t' \leq \omega \leq 4t - 4t'$.

It should be emphasized that a negative second-neighbor hopping t' suffices to give the correct tendency to the following: (a) The Hall coefficient, which is positive for the open orbits encountered at small doping and changes sign at large doping when the orbits close

sufficiently. (b) The doping dependence of the uniform magnetic susceptibility. Indeed, in this noninteracting limit the latter quantity is simply a measure of the density of states which here clearly increases with hole doping (Fig. 3) instead of decreasing as in the nearest-neighbor model. (c) The temperature dependence of the magnetic susceptibility which does have a maximum at progressively lower temperature as the doping increases [Fig. 3(b)]. Other quantities have also been discussed in Ref. 5, for example. Although there is no quantitative agreement with experiment in this noninteracting limit, at least the tendencies and signs of the effects are correct, contrary to the model with $t'=0$ which, in the noninteracting limit, has the wrong sign for all the effects mentioned above.

As can be seen from Fig. 2(a) there is no nesting at half filling so that, unlike the usual $t'=0$ case, it is not obvious whether in the finite negative t' case there is antiferromagnetism at this filling. In fact, antiferromagnetism does appear for negative t' as long as U is sufficiently large, and t' is larger than $-0.25t$. (See Ref. 33 and Sec. III A).

We will be mostly interested in the imaginary part of the magnetic susceptibility $\chi''(\mathbf{q}, \omega)$, as measured by magnetic neutron scattering. In two dimensions, this quantity is particularly sensitive to band-structure effects as noted before.[3,30] In the zero-temperature noninteracting limit, we have ($\mu_B = 1$, $k_B = 1$, $\hbar = 1$, $S = \frac{1}{2}$ and in all the figures, but not the equations, $t = 1$)

$$\chi_0''(\mathbf{q}, \omega) = 1/(8\pi) \int_{-\pi}^{\pi} dk_x \int_{-\pi}^{\pi} dk_y \, \delta[\omega - \varepsilon(\mathbf{k}+\mathbf{q}) + \varepsilon(\mathbf{k})] \{ f[\varepsilon(\mathbf{k}) - \mu] - f[\varepsilon(\mathbf{k}+\mathbf{q}) - \mu] \} \tag{4}$$

(a)

———— $\mu = -0.32$
············· $\mu = -0.66$
- - - - $\mu = -1.28$

(b)

———— $\mu = 4t' = -0.64$
- - - - $\mu = \mu_c^- = -1.09$
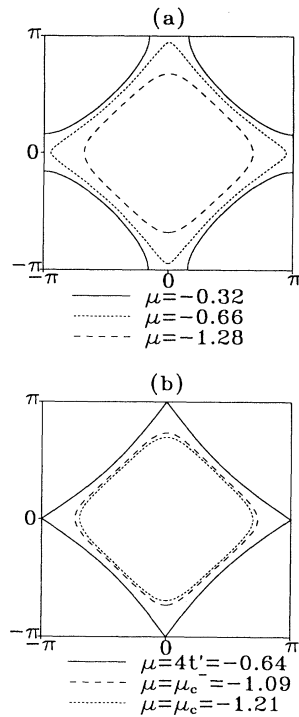············· $\mu = \mu_c = -1.21$

FIG. 2. (a) Three types of Fermi surfaces encountered when second-neighbor hopping t' is in the range $-0.5t < t' < 0$. The specific case plotted is $t' = -0.16t$. Near half filling the orbits are open (solid line), then as the system is doped they close, but there is a change in curvature as one goes around the Fermi surface (short-dashed line). Finally, the Fermi surface is closed and has a single curvature (dashed line). (b) Limiting orbits between the three types of cases identified in (a). The solid line is at the boundary between open and closed orbits and corresponds to the Fermi surface lying at the Van Hove singularity. The long-dashed line is at a bare chemical potential μ_c^- [see Eq. (20)] where the change in curvature of the Fermi surface, as seen from (q_x, π) scans, is no longer observable. The short-dashed line is at a bare chemical potential μ_c [see Eq. (B7)] where the change in curvature of the Fermi surface disappears, as seen from (q, q) scans.
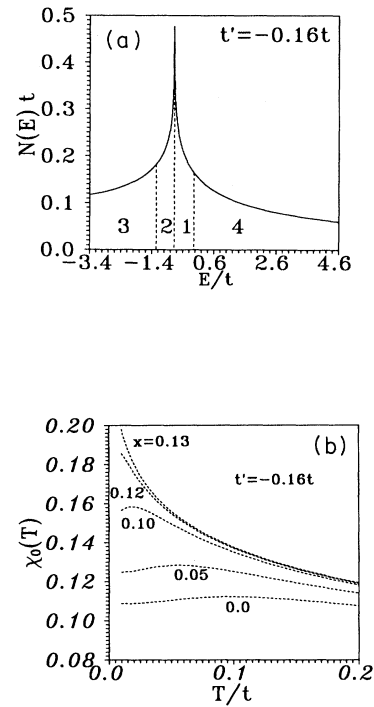

FIG. 3. (a) Density of states when $t' = -0.16t$. [See Eq. (3)]. When the Fermi level lies in region 1, orbits are open, in region 2 they are closed but there is a change of curvature, and when the Fermi level is in region 3 the Fermi surface has a single curvature. When the Fermi level is in region 4, orbits are open and a kinetic gap reappears in the magnetic structure factor around (π, π), as is the $t' = 0$ model. (b) Uniform magnetic susceptibility of the noninteracting system when $t' = -0.16t$. Clearly this is a better perturbative starting point than the $t' = 0$ model since the magnetic susceptibility increases upon doping and the maximum in the temperature dependence moves to lower temperatures as observed experimentally. The temperature scale for the maximum is also small. The increase in the magnetic susceptibility upon doping is easy to understand from the fact that in region 1 in (a) the density of states increases upon hole doping.

where $f[\varepsilon(\mathbf{k})-\mu]$ is the Fermi-Dirac distribution. For the ideal case of a circular Fermi surface with dispersion relation $\omega=k^2/2$, we have,

$$\chi_0''(\mathbf{q},\omega)=1/(4\pi q^2)\{\sqrt{2\mu q^2-[\omega-(q^2/2)]^2}$$
$$-\sqrt{2\mu q^2-[\omega+(q^2/2)]^2}\} \ . \tag{5}$$

In the above result, Θ functions which insure positivity of the arguments of the square roots should appear. To simplify the notation, we adopt from now on the convention that a term vanishes whenever it contains a square root with a negative argument. In the limit $|\omega|\ll|\mu-q^2/8|$ we may write,

$$\lim_{\omega\to 0}\lim_{\omega\ll|\mu-q^2/8|}\frac{\chi_0''(\mathbf{q},\omega)}{\omega}=\frac{1}{4\pi\sqrt{2}q}\frac{1}{[\mu-q^2/8]^{1/2}} \ .$$
$$\tag{6}$$

Figure 4 illustrates how this square-root singularity develops as the zero-frequency limit is approached. Clearly the singularity near $q=2k_F$ is a signature of the Fermi surface. Because of the restriction $|\omega|\ll|\mu-q^2/8|$, however, it is important to notice that the maximum in $\chi_0''(\mathbf{q},\omega)/\omega$ near $2k_F$ grows, in fact, as $1/\sqrt{\omega}$. The singularity (6) in $\chi_0''(\mathbf{q},\omega)/\omega$ is basically the two-dimensional version of the physics which eventually leads to Kohn anomalies in phonon dispersion relations The shape of $\chi_0''(\mathbf{q},\omega)$ near $2k_F$ in Fig. 4, a $2k_F$ anomaly, is characteristic of the two-dimensional circular Fermi surface and will be encountered in the lattice case as well. The two-dimensional results are contrasted with one and three dimensions in Appendix A.

Anticipating results which will be discussed in more detail later, consider now the usual one-band nearest-neighbor problem, with the well-known "rounded-

square" Fermi surface. The result for $\chi_0''(\mathbf{q},\omega)$ may be computed analytically, as shown in Appendix A. The low-frequency limit of this result is illustrated in Fig. 5(a) along the high-symmetry directions for a doping $x=0.14$. Since the length of the vector joining opposite pieces of the Fermi surface depends on direction, one notices that in each of the three directions considered, there is a distinct large-q square-root singularity. The strength of the singularity in $\chi_0''(\mathbf{q},\omega)$ in Fig. 5(a) is twice as large along the zone edge as it is along the diagonal direction. (See Appendix A.) The $(0,0)$ to $(0,\pi)$ direction is special because the corresponding vector is larger than π and hence it folds back in the first Brillouin zone, corresponding physically to *umklapp* scattering. In an extended zone scheme, this singularity (indicated by arrow number two in the figure) corresponds to scattering between the two rounded corners of adjacent Fermi surfaces. This picture is confirmed by the fact that the curvature in $\chi_0''(\mathbf{q},\omega)$ is in a direction opposite to that found in the circular Fermi surface case of Fig. 4. In fact, close to the singularities, the shape of $\chi_0''(\mathbf{q},\omega)$ is always similar to the case of the circular Fermi surface, except in the cases where *umklapp* scattering or holelike effects produce a mirror image.

It is important to remember that in higher dimensions $\chi_0''(\mathbf{q},\omega)$ decreases monotonically towards $2k_F$, leaving interactions mostly responsible for structure which may appear in the magnetic structure factor. By contrast, in two dimensions this is not the case: Interactions mostly modulate the intensity of various sharp features which are already present in the noninteracting limit [Figs. 5(b)
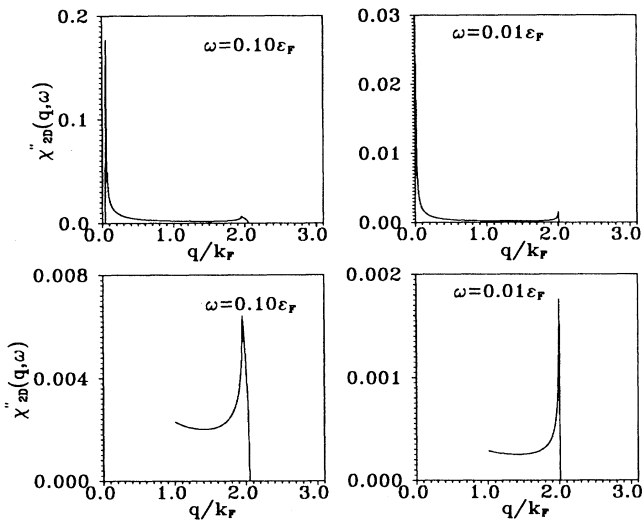

FIG. 4. Imaginary part of the spin susceptibility for free two-dimensional fermions. One sees in the top two panels that as the frequency decreases, the feature at $q=2k_F$ sharpens. This is more clearly seen in the lower two panels which show an enlargement of the two corresponding $q=2k_F$ regions.
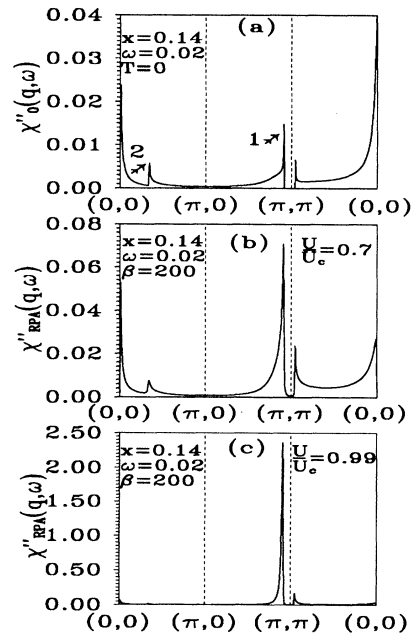
FIG. 5. Imaginary part of the spin susceptibility for the nearest-neighbor one-band Hubbard model. (a) Exact result for the Lindhard function (see Appendix A). (b) and (c) were computed for the parameters indicated in the figure on 1000×1000 lattices with Lorentzian energy-level broadening $\eta=0.02t$.

and 5(c)]. These singularities, or lattice-$2k_F$ anomalies, should appear in magnetic neutron scattering as clear signatures of the Fermi surface. In the noninteracting, zero-frequency limit, the strength of the singularity at a given q is generally largest when the curvature of pieces of the Fermi surfaces joined by this q is smallest. This is quite different from nesting, which occurs when a given q maps a finite segment of the Fermi surface into another. Nevertheless, we will designate the q with the *largest* singularity (largest lattice-$2k_F$ anomaly) as the *pseudonesting* vector since nesting is recovered in the limit of zero curvature of the Fermi surface. The beginning of the next section expands on this concept of pseudonesting, and classifies all possible types of singularities in the noninteracting limit.

III. MAGNETIC STRUCTURE FACTOR FOR $U=0$, IN THE $T \to 0$ LIMIT

In general, the magnetic structure factor is obtained from χ'', the imaginary part of the spin susceptibility, through the fluctuation-dissipation theorem:

$$S_0(\mathbf{q},\omega) = 2 \frac{\chi_0''(\mathbf{q},\omega)}{[1 - \exp(-\beta\omega)]} . \qquad (7)$$

Given the importance of the noninteracting limit in determining the position of the peaks, we consider it first. Taking the zero-frequency limit, and expanding in powers of ω in the most direct manner leads to the following asymptotic behavior for the structure factor of the noninteracting system:

$$S_0(\mathbf{q}) \simeq \frac{\max(T,\omega)}{4\pi} \int_{-\pi}^{\pi} dk_x \int_{-\pi}^{\pi} dk_y \delta[\varepsilon(\mathbf{k}) - \varepsilon(\mathbf{k}+\mathbf{q})]$$

$$\times \delta[\varepsilon(\mathbf{k}) - \mu]$$

$$\text{if } \min(T,\omega) \ll \max(T,\omega) \ll |\mu| . \qquad (8)$$

The same kind of expansion leads to the asymptotic result for $\chi''(\mathbf{q},\omega)/\omega$ discussed in Sec. II. Hence, the above expression is also valid in the same limit, in particular, the square-root singularities in the wave vector that will be encountered later should be interpreted in the manner discussed in Sec. II: even at $T=0$, the frequency leads to a cutoff as long as it is finite.

When $t'=0$, the asymptotic result, Eq. (8), becomes incorrect also when the temperature or the frequency become comparable to the absolute value of the chemical potential, taken as zero at half filling. For temperatures much higher than $|\mu|$, thermal excitations are spread over an energy interval of order $T > |\mu|$ around the Fermi energy μ and the bare structure factor becomes quite insensitive to the value of the chemical potential, behaving essentially as if $|\mu|$ were zero. In this case the imaginary part of the bare susceptibility is largest when q is close to $\mathbf{Q}_{AF} = (\pi,\pi)$ (the null wave vector notwithstanding) and obeys a MFL-type of scaling,[32] that is,

$$(\pi/4)N(\omega/2) \frac{\sinh(\beta\omega/2)}{\cosh(\beta\mu) + \cosh(\beta\omega/2)}$$

$$\to (\pi/4)N(\omega/2)\tanh(\beta\omega/4) , \qquad (9)$$

where $N(\varepsilon)$ is the single-spin density of states. This is the regime of nested Fermi liquids discussed by Ruvalds and Virosztek.[20] The corresponding discussion when $t' \neq 0$ is more complex, so it is reported in Sec. III B 2.

It is also instructive to rewrite (8) for the structure factor as

$$S_0(\mathbf{q}) \simeq \frac{\max(T,\omega)}{2\pi} \int_{-\pi}^{\pi} dk_x \int_{-\pi}^{\pi} dk_y \delta\{[\varepsilon(\mathbf{k}+\mathbf{q}) - \mu] + [\varepsilon(\mathbf{k}) - \mu]\}\delta[\varepsilon(\mathbf{k}) - \varepsilon(\mathbf{k}+\mathbf{q})]$$

$$\text{for } \min(T,\omega) \ll \max(T,\omega) \ll |\mu| . \qquad (10)$$

In this form, it is apparent that the structure factor will depend on how the condition $\xi(\mathbf{k}+\mathbf{q}) = -\xi(\mathbf{k})$ is satisfied $[\xi(\mathbf{k}) \equiv \varepsilon(\mathbf{k}) - \mu]$. When this condition is satisfied for a finite range of $\mathbf{k}$, we have nesting. At the edge of the $2k_F$ anomaly, the Fermi surface is displaced by a vector q such that it becomes tangent to the original Fermi surface instead of intersecting it at two points. The smallest curvatures tend to give the largest singularity, what we call pseudonesting. Mathematically, this may also be seen by changing variables in the previous equation so that

$$S_0(\mathbf{q}) \simeq \frac{\max(T,\omega)}{4\pi} \sum_i \frac{1}{|\nabla_{\mathbf{k}_i}\varepsilon_{\mathbf{k}_i - \mathbf{q}/2} \times \nabla_{\mathbf{k}_i}\varepsilon_{\mathbf{k}_i + \mathbf{q}/2}|}$$

$$\text{for } \min(T,\omega) \ll \max(T,\omega) \ll |\mu| , \qquad (11)$$

where the sum extends over the set of distinct points $\mathbf{k}_i$ in the first Brillouin zone such that for a given q, $\varepsilon_{\mathbf{k}-\mathbf{q}/2} = \varepsilon_{\mathbf{k}+\mathbf{q}/2}$ with both $\mathbf{k}-(\mathbf{q}/2)$ and $\mathbf{k}+(\mathbf{q}/2)$ on the Fermi surface $(\varepsilon_{\mathbf{k}-\mathbf{q}/2} + \varepsilon_{\mathbf{k}+\mathbf{q}/2} = 2\mu)$. The Jacobian has been written in a form which makes it clear that when $\mathbf{q} = \mathbf{q}_0$ joins two points of the Fermi surface whose tangents are parallel, the cross product vanishes, leading to a singularity in the structure factor. There are three different types of such wave vectors $\mathbf{q}_0$. The first type is the trivial null wave vector which maps the Fermi surface onto itself. The second type consists of the wave vectors $\mathbf{q}_0$ that connect pairs of parity-related points of the Fermi surface. Since for these points q has to cross the origin $(0,0)$, these wave vectors (and their *umklapp*) are defined by the equations $\varepsilon(\mathbf{q}_0/2) = \mu$, $\varepsilon[\mathbf{q}_0/2 + (\pi,\pi)] = \mu$, $\varepsilon[\mathbf{q}_0/2 + (\pi,0)] = \mu$, $\varepsilon[\mathbf{q}_0/2 + (0,\pi)] = \mu$. Finally the last

type of wave vector only occurs when the curvature of the Fermi surface changes sign. These wave vectors link tangent points of the Fermi surface without going through (0,0). This type of solution will occur for a range of values of μ when $t' \neq 0$. However, if $t' = 0$, the curvature of the Fermi surface is always the same, so in this case the maxima of the bare structure factor are at $\mathbf{q}_0 = 0$, $\cos(q_{0x}/2) \pm \cos(q_{0y}/2) = \mu/2t$, and $\cos(q_{0x}/2) \pm \cos(q_{0y}/2) = -\mu/2t$.

To continue our discussion of pseudonesting, it is instructive to find the functional form of the singularities near the vectors $\mathbf{q}_0$. This may be done by expanding Eq. (11) around $\mathbf{q}_0$. For infinitesimal displacements from $\mathbf{q}_0$, the shape of the pieces of Fermi surfaces which touch can, in general, be approximated by circles. Define a displacement $\Delta \mathbf{q}$, measured from the point where the two circles are tangent, and a unit vector $\hat{\mathbf{p}}$ parallel to the line joining the two centers of the circles when they just touch (at $\mathbf{q}_0$). To fix a sign convention, it suffices to think of one of the circles as fixed when the other is moved by $\Delta \mathbf{q}$. Then, we take the direction of $\hat{\mathbf{p}}$ pointing from the center of the circle which will be displaced towards the center of the fixed circle. In the simplest case, $\Delta \mathbf{q}$ is along $\hat{\mathbf{p}}$ and one obtains, away from the Van Hove singularities,

$$S_0(\mathbf{q}_0 + \Delta \mathbf{q}) \simeq \frac{\max(T,\omega)}{2\pi v_+ v_-} \left[\frac{R_+ R_-}{R_+ + R_-} \right]^{1/2} \frac{1}{\sqrt{2|\Delta \mathbf{q}|}} \; ,$$

$$(12a)$$

where $v_\pm$ are the Fermi velocities at, respectively, $\varepsilon_{\mathbf{k}+\mathbf{q}/2}$ and $\varepsilon_{\mathbf{k}-\mathbf{q}/2}$ while $R_\pm$ are the absolute value of the k-space radii of curvature of the Fermi surface at the corresponding points. Note that $S_0(\mathbf{q}_0 + \Delta \mathbf{q}) = 0$ when $\Delta \mathbf{q}$ points in the direction opposite to $\hat{\mathbf{p}}$. The functional form of the singularity is the same as in the case of free electrons in a continuum, where $R_+ = R_-$, $v_+ = v_-$. These two equalities are also satisfied, in general, when $\mathbf{q}_0$ is a vector that

connects parity-related points of the Fermi surface. Clearly, the strength of the singularity depends on the radius of curvature of the Fermi surface at this point, as we stated above. When the Fermi surface exhibits changes in curvature, it is, in principle, possible to find situations where $R_+ \neq R_-$, but this situation is not encountered in the high-symmetry directions considered in the rest of this paper.

For an infinitesimal displacement $\Delta \mathbf{q}$ along an arbitrary direction, define ψ as the angle between the vectors $\Delta \mathbf{q}$ and $\hat{\mathbf{p}}$. As long as $\cos\psi \gg |\Delta \mathbf{q}|/(2R_+ + 2R_-)$, we find,

$$S_0(\mathbf{q}_0 + \Delta \mathbf{q})$$

$$\simeq \frac{\max(T,\omega)}{2\pi v_+ v_-} \left[\frac{R_+ R_-}{R_+ + R_-} \right]^{1/2} \frac{1}{\sqrt{2|\Delta \mathbf{q}| \cos\psi}} \; . \quad (12b)$$

Otherwise, $S_0(\mathbf{q}_0 + \Delta \mathbf{q})$ vanishes. This last result is just another way of saying that just the component of displacement $\Delta \mathbf{q}$ along $\hat{\mathbf{p}}$ contributes.

At first sight, it seems that while the presence of the lattice allows umklapp processes and pseudonesting, the functional form of the singularity is always $1/\sqrt{|\Delta \mathbf{q}|}$. In fact, the lattice allows one more possibility when there are changes of curvature in the Fermi surface. Indeed, as discussed after Eq. (11), it becomes possible in this case to find certain singular $\mathbf{q}_0$ where the Fermi surfaces which become tangent are curved in the same direction, contrary to the last case (12b) where they were curved in opposite directions. (See Appendix B and vector $\mathbf{Q}_3$ in Fig. 21 for an example.) We define $\hat{\mathbf{p}}$ as above. We then obtain, for a general displacement $\Delta \mathbf{q}$ away from $\mathbf{q}_0$,

$$S_0(\mathbf{q}_0 + \Delta \mathbf{q}) \simeq \frac{\max(T,\omega)}{2\pi v_+ v_-} \frac{1}{[-2|\Delta \mathbf{q}| \cos\psi (|R_+ - R_-|/R_+ R_-) + (|\Delta \mathbf{q}| \sin\psi)^2/R_+ R_-]^{1/2}} \; . \qquad (12c)$$

We obtain zero when the argument of the square root is negative. It is clear that, when $\psi = \pi/2$, or when $R_+ = R_-$, a new $1/|\Delta \mathbf{q}|$ type of singularity is encountered. In fact, when $R_+ = R_-$, the direction $\hat{\mathbf{p}}$ is not defined, and we should take $\psi = \pi/2$ in the above expression. (In the perfectly circular Fermi surface case, this type of $1/|\Delta \mathbf{q}|$ singularity occurs only for $\mathbf{q}_0 = 0$.) As discussed in Appendix B, this new type of singularity is encountered when $t' \neq 0$ for a certain range of fillings.

Obviously, still more singular behavior of $S_0(\mathbf{q}_0 + \Delta \mathbf{q})$ is possible when the pieces of Fermi surfaces which touch become parallel over some range. This possibility is encountered when $t' = 0$, $\mu = 0$, and for $t' < -0.5t$, a case not discussed here.

A. Bare structure factor
with nearest-neighbor hopping only

1. Zero-frequency limit

For frequencies less than $2|u|$ and $t' = 0$, there are two remarkable sets of lattice-$2k_F$ anomalies. One with four equivalent wave vectors centered about the origin (0,0) and the other one, also with four equivalent wave vectors, centered about the antiferromagnetic wave vector $\mathbf{Q}_{AF}$. It is the latter feature which has been observed experimentally in detail,[6,7] and this is the one we will concentrate on. However, as will be discussed in more detail later, the relative size of the small and large wave-vector lattice-$2k_F$ anomalies could be a way to confirm or re-

ject[23] the MFL suggestion that one must consider the physical system as being far from a magnetic instability.[30,32]

Equation (11) can be solved exactly for arbitrary q.

The result is written in the following form, using again the convention that there are implicit Θ functions which lead to the vanishing of any term which would lead to an imaginary number:

$$S(\mathbf{q}) = \frac{\max(T,\omega)}{16\pi t^2} \frac{[\sin(q_x/2)\sin(q_y/2)]^{1/2}}{\{[(\mu/2t)\sin(q_x/2)\sin(q_y/2)]^2+[\cos^2(q_x/2)-\cos^2(q_y/2)]^2\}^{1/2}}$$
$$\times \left[\frac{1}{[(1-x_+^2)(1-y_-^2)]^{1/4}}+\frac{1}{[(1-x^2)(1-y_+^2)]^{1/4}}\right], \tag{13a}$$

where

$$x_\pm = \frac{(\mu/2t)\cos(q_x/2)\sin^2(q_y/2)\pm\cos(q_y/2)\{[(\mu/2t)\sin(q_x/2)\sin(q_y/2)]^2+[\cos^2(q_x/2)-\cos^2(q_y/2)]^2\}^{1/2}}{\cos^2(q_y/2)-\cos^2(q_x/2)}, \tag{13b}$$

$$y_\pm = \frac{(\mu/2t)\cos(q_y/2)\sin^2(q_x/2)\pm\cos(q_x/2)\{[(\mu/2t)\sin(q_y/2)\sin(q_x/2)]^2+[\cos^2(q_x/2)-\cos^2(q_y/2)]^2\}^{1/2}}{\cos^2(q_x/2)-\cos^2(q_y/2)}. \tag{13c}$$

Note that Eq. (13) is ill-behaved when q_x or q_y is zero and when q_x is equal to q_y. The limiting behavior in these two special cases are, respectively,

$$S_0(q,0) = \frac{\max(T,\omega)}{16\pi t^2 \sin(q/2)} \left[\frac{1}{\{1-[\cos(q/2)-\mu/2t]^2\}^{1/2}}+\frac{1}{\{1-[\cos(q/2)+\mu/2t]^2\}^{1/2}}\right] \tag{14a}$$

and

$$S_0(q,q) = \frac{\max(T,\omega)}{4\pi t} \frac{\cotan(q/2)}{|\mu|} \frac{1}{\sqrt{\cos^2(q/2)-\mu^2/16t^2}}. \tag{14b}$$

For the $t'=0$ limit, the Hubbard model has particle-hole symmetry, so the results are valid for both hole doping and electron doping. Near the antiferromagnetic wave vector the maximum of the structure factor is located on the zone edge, hence we set q_y to π. Equation (13) then reduces to

$$S_0(q_x,\pi) = \frac{\max(T,\omega)}{8\pi t^2} \frac{1}{[\cos^2(q_x/2)-(\mu/2t)^2]^{1/2}[\cos^2(q_x/2)+(\mu/2t)^2\tan^2(q_x/2)]^{1/2}}, \tag{15}$$

where $0 \leq q_x \leq \pi$, $|\mu| \leq 2t$, and $T,\omega \ll |\mu|$.

Thus, asymptotically close to zero temperature and zero frequency, the bare structure factor has the largest square-root singularity at the pseudonesting wave vectors[21,23] $\mathbf{Q}_n$, located at $\{[\pm 2\cos^{-1}(-\mu/2t),\pi], [\pi,\pm 2\cos^{-1}(-\mu/2t)]\}$, as illustrated in Fig. 6. As discussed in Sec. II, this square-root singularity is characteristic of two-dimensional systems.

Equation (15) also shows that close to the antiferromagnetic wave vector, the bare structure factor has a gap in q space for wave vectors greater than the pseudonesting wave vector. Geometrically the gap simply means that wave vectors of the form $(\pm q_x,\pi)$ with q_x larger than $2\cos^{-1}(-\mu/2t)$ cannot be fit inside the Fermi surface. This gap is the extension in q space of the *kinetic gap* discussed by Bulut and Scalapino.[17] The small wavevector lattice-$2k_F$ anomalies discussed earlier are located at $\{[\pm 2\cos^{-1}(1-|\mu|/2t),0], [0,\pm 2\cos^{-1}(1-|\mu|/2t)]\}$ as can be seen from Eq. (14a).

2. Frequency dependence

Since χ'' is an odd function of frequency, we consider only positive values of ω without loss of generality. From the energy conservation constraint in Eq. (4) it can be shown that the imaginary part of the susceptibility χ'' is zero for frequencies greater than

$$\widetilde{\omega}_+ = 4t[\sin(q_x/2)+\sin(q_y/2)]. \tag{16}$$

At zero temperature the Fermi-Dirac distributions become Θ functions, which force $\chi_0''(q_x,\pi;\omega)$ to vanish also for wave vectors q_x greater than q_x^c,

$$q_x^c(\omega) = 2\cos^{-1}\left[-\frac{\mu}{2t}-\frac{\omega}{4t}\right] \tag{17}$$

if $\mu < 0$. At $\mathbf{Q}_{AF}=(\pi,\pi)$, the imaginary part of the susceptibility is thus zero for frequencies less than $2|\mu|$, as shown by Bulut and Scalapino.[17] Thus, Eq. (17) defines
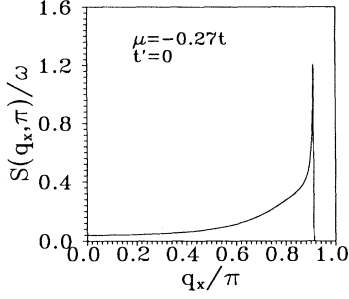
FIG. 6. Limiting value of the bare structure factor $S_0(q_x)$ divided by ω as a function of q_x for $q_y = \pi$ (see Eq. (15)]. Doping is $x = 0.14$. One can see the kinetic gap and near that gap the same square-root singularity as in the free-fermion case (Sec. II and Fig. 4).

the boundary of the extension of their *kinetic gap* into the $(q_x, q_y = \pi; \omega)$ plane. The full boundary of the kinetic gap in the region $\omega \geq 0$ is simply

$$\tilde{\omega}_- = \max\left\{0, -4t\left|\cos\left[\frac{q_x}{2}\right] + \cos\left[\frac{q_y}{2}\right]\right| - 2\mu\right\} \quad (18)$$

for $\mu < 0$. In other words, in the positive-frequency region, when ω is less than $\tilde{\omega}_-$, $\chi_0''(q_x, q_y, \omega)$ vanishes at zero temperature. We will refer to this region simply as the "kinetic gap." It fills in slowly as the temperature is increased, and disappears when the temperature is of order $2|\mu|$. This kinetic gap may correspond to the "spin gap" in the neutron-scattering literature.[11,9] It plays a key role for the collective mode described in Sec. III and survives in certain cases even in the presence of second-neighbor hopping.

The full frequency and momentum dependence of the zero-temperature bare structure factor can be calculated exactly for any wave vector, but, in general, a quartic equation must be solved. We thus restrict ourselves to work along the three high-symmetry directions $(q,0)$, (q,q), and (q,π) (Figs. 5 and 7) where only a quadratic equation needs to be solved to express the result in terms of elliptic integrals (Appendix A and Ref. 25). The frequency dependence of the Q_{AF} and Q_n directions are of particular interest to us. As mentioned by Bulut and Scalapino,[17] the structure factor at (π,π) is simply

$$1/(16\pi)\Theta(\omega - 2|\mu|)K(\{1 - [\omega/(8t)]^2\}^{1/2}),$$

where $K(x)$ is the complete elliptic integral of the first kind. At the pseudonesting wave vector Q_n, as long as $\mu \neq 0$, the maximum in the structure factor is proportional to the square root of the frequency $S_0(Q_n, \omega) \approx t^{-1}(\omega/|\mu|)^{1/2}$ if $\omega \ll |\mu|$. This $\omega^{1/2}$ dependence is the same as that discussed in the circular Fermi surface case in Sec. II. When $\mu = 0$, (π, π) is a nesting vector and the bare structure factor drops abruptly to zero at $\omega = 0$.

Other than the Fermi energy, when $t' = 0$ the energy scale introduced by band-structure effects close to $q = Q_{AF}$ is equal to $2|\mu|$, which corresponds to twice the difference between the Fermi energy at half filling, and the Fermi energy at the filling of interest. For the experi-

mentally relevant dopings, this is an energy scale five to ten times larger than the observed scale of about 150 K.

B. Bare structure factor
with next-nearest-neighbor hopping

1. Zero-frequency limit

The energy spectrum of the tight-binding Hamiltonian with a next-nearest-neighbor hopping term is given by Eq. (2). We work with t' negative in the above expression because this corresponds to the sign suggested by LDA calculations.[14] The case of positive t' is also covered since, for a bipartite lattice, the canonical particle-hole transformation $c_{i\sigma} \rightarrow (-1)^p c_{i\sigma}^+$ ($p = 1$ on one sublattice, and $p = 0$ on the other) maps the Hamiltonian onto itself with a change of sign of both t' and μ. We only consider cases where the hopping amplitude $|t'|$ is less than $t/2$ in order to avoid any change in the symmetry axes of the Fermi surface.

Next-nearest-neighbor hopping alters the curvature of the Fermi surface for values of the chemical potential close to zero. It also changes the dependence of the chemical potential on the density of electrons. The bare structure factor in the low-frequency limit can, in princi-
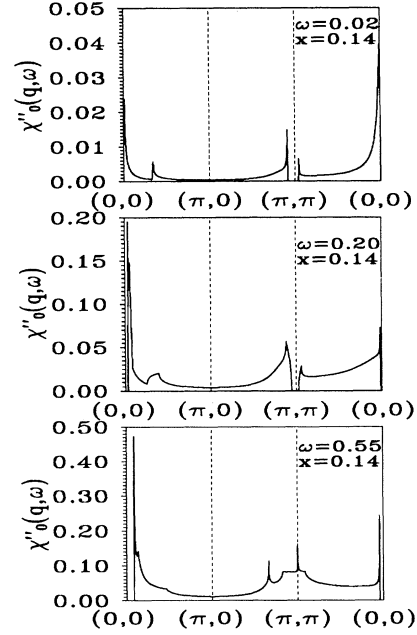

FIG. 7. Exact result χ'' for two-dimensional tight-binding electrons along the highly symmetric directions $(q,0)$, (q,π), and (q,q). Energy is measured in units of t. On the top graph there is an *umklapp* lattice $2k_F$ anomaly in the $(q,0)$ direction in addition to the lattice $2k_F$ anomaly at $(\pi \pm \delta\pi, \pi)$. One also sees that there is a region of $\mathbf{q}$ near (π, π) where $\chi''(\mathbf{q}, \omega)$ vanishes, allowing the existence of a collective mode. The middle panel shows that the peaks broaden as ω increases at the same time as the kinetic gap decreases around $\mathbf{q} = (\pi, \pi)$. In the bottom panel, one sees that the (π, π) point becomes the maximum when $\omega > 2\mu$, as in the numerical calculation of Fig. 11.

ple, be calculated for any wave vector **q** but the result involves solving a quartic equation, except along the three high-symmetry axes $(q,0)$, (q,q), and (q,π). In the present section, we restrict ourselves to the direction (q,π). Results for the other two high-symmetry directions also contain rich information on the structure of the Fermi surface, as shown in Appendix B. Setting $q_y = \pi$ we obtain

$$S_0(q_x,\pi) = \frac{\max(T,\omega)}{8\pi t^2} \frac{1}{\{(1-t'\mu/t^2)^2 \cos^2(q_x/2) - [4t'(\mu-4t')/t^2]\sin^2(q_x/2)\}^{1/2}}$$

$$\times \left\{ \frac{1+(2t'/t)A^- \cos(q_x/2)}{([1-(A^-)^2]\{[1+(2t'/t)A^- \cos(q_x/2)]^2 - [1-(A^-)^2]\sin^2(q_x/2)\})^{1/2}} \right.$$

$$\left. + \frac{1+(2t'/t)A^+ \cos(q_x/2)}{([1-(A^+)^2]\{[1+(2t'/t)A^+ \cos(q_x/2)]^2 - [1-(A^+)^2]\sin^2(q_x/2)\})^{1/2}} \right\}$$

(19a)

for $0 < q_x < \pi$, and where $A^{\pm}$ is given by

$$A^{\pm} = - \left[1 + \frac{t'\mu}{t^2} \right] \frac{t}{4t'} \cos\left[\frac{q_x}{2} \right]$$

$$\pm \frac{t}{4t'} \left[\left[1 - \frac{t'\mu}{t^2} \right]^2 \cos^2\left[\frac{q_x}{2} \right] \right.$$

$$\left. - \frac{4t'(\mu-4t')}{t^2} \sin^2\left[\frac{q_x}{2} \right] \right]^{1/2}$$

(19b)

The contribution of any term above vanishes for any combination of μ, q_x, or t' that makes this term imaginary. The structure factor may exhibit several singularities due to the geometry of the Fermi surface. Since the latter depends on the chemical potential, its low-temperature behavior can be characterized by three doping regimes when $\mu < 0$, as illustrated in Fig. 8.

The first regime, close to $\mu = 0$ $(0 > \mu > 4t')$ in Fig. 8(a), is characterized by the absence of a pseudogap and the presence of a lattice-$2k_F$ anomaly at the wave vector $\mathbf{q}_0 = \{2\cos^{-1}[-\mu/(2t)],\pi\}$ and symmetry-related points. The peak is a square-root singularity as usual but inverted because of the holelike nature of the Fermi surface. The absence of a kinetic gap in this doping regime can be easily explained in terms of the Fermi surface geometry. For these values of μ, the Fermi surface is open, as shown in the inset, which allows for the possibility of joining different sections of the Fermi surface with wave vectors larger than the $t' = 0$ pseudonesting vectors along the $(q_x, q_y = \pi)$ direction. When the chemical potential decreases from its half-filling value, the intensity at (π,π) increases, as shown by the dotted line in Fig. 8(a), until the chemical potential eventually reaches $4t'$, as in Fig. 8(b). At this point, the Fermi surface closes, touching the Brillouin zone at the points $(\pm\pi,0)$ and $(0,\pm\pi)$ which lead to Van Hove singularities in the density of states. These points are linked together by the four vectors $\mathbf{Q}_{AF} = (\pm\pi,\pm\pi)$. There is thus a strong divergence in the structure factor at $\mathbf{Q}_{AF}$ because of the vanishing Fermi velocities [Eq. (11) fails in this limit]. A small peak remains at $q_x = q_x^0$ because of a remaining lattice-$2k_F$ anomaly.

A second regime, Fig. 8(c), occurs when the chemical potential is lowered below $4t'$ but is still larger than

$$\mu_c^- \equiv -\frac{t^2}{2t'} - \left[\left[\frac{t^2}{2t'} \right]^2 + 8t^2 \right]^{1/2}.$$

(20)

(Note that $\mu_c^- < 4t'$ for $|t'| < t/2$.) For such values of μ
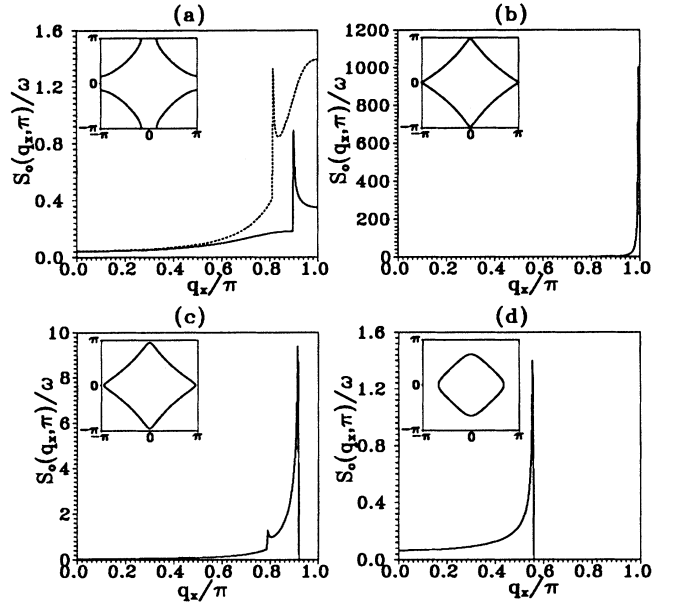

FIG. 8. Wave-vector dependence of the bare structure factor divided by frequency at asymptotically low temperature along the line $q_y = \pi$ for $t' = -0.16t$ [Eq. (19)]. The four regions correspond to the three Fermi surface shapes discussed in Fig. 2(a) and to the limiting case where the Fermi surface is at the Van Hove singularity. The insets show the corresponding Fermi surfaces. The chemical potentials used for the solid lines are, respectively, in units of $t = 1$, -0.32, -0.64, -0.66, and -1.28, in the direct corresponding to those used in the other two high-symmetry directions discussed in Appendix B (Figs. 18 and 19). In (a) there is also a dotted line, computed for $\mu = -0.58$, which is also in the open-orbit case. This is closer to the Van Hove singularity so that weight starts to build up at (π,π). In (b), the large peak at (π,π) is extremely sensitive to temperature and frequency.

the Fermi surface is closed, and the size of the q_x component of the wave vectors that can be fitted inside the Fermi surface is limited by its diameter. Thus, a gap opens up at a wave vector $\mathbf{Q}_n^1$ (and those related by square symmetry):

$$q_x^1 = 2\cos^{-1}\left[\left[\frac{4t'(\mu-4t')}{[t+(t'/t)\mu]^2-16t'^2}\right]^{1/2}\right], \quad q_y^1 = \pi$$

(21)

for which the bare structure factor is singular. The anomaly at q_x^0 is still present. There are two divergences because there is both positive and negative curvature in the Fermi surface.

Finally, in the third regime, when the chemical potential is lowered below μ_c^-, as in Fig. 8(d), the structure factor along the direction (q_x,π) is not sensitive to the existence of two curvatures, even though the two curvatures persist for a range of smaller fillings. (As shown in Appendix B, the diagonal direction is the one which is most sensitive to the existence of two curvatures in the Fermi surface.) In this regime the structure factor behaves similarly to the $t'=0$ limit with a singularity at $\mathbf{Q}_n$.

For finite t', the system is electron doped even at zero chemical potential. For positive values of the chemical potential, the Fermi surface is composed of disconnected sections such that, in the direction (q_x,π), q_x must be greater than π in order to link two sections of the Fermi

surface [region 4 in Fig. 2(a)]. In an extended zone scheme, sections of the Fermi surfaces are actually closed around all points in k space equivalent to (π,π). Since there is no change in the curvature of the Fermi surface, we should not expect two structures in $S_0(q_x,\pi)$. The structure factor will behave similarly to the limit $t'=0$, with a singularity at $\mathbf{Q}_n$ and a gap for larger values of q_x.

In summary, the effect of a next-nearest-neighbor hopping term is mainly felt for values of the chemical potential larger than μ_c^- up to about $\mu=0$. The fact that the particle-hole symmetry of the Hubbard model is broken when next-nearest-neighbor hopping is allowed is clearly reflected in the bare structure factor, hole doping (negative values of μ) being more sensitive to t' than electron doping (which involves mainly positive values of μ but also a small range of negative values of μ, between roughly $2t'$ and 0).

2. Frequency dependence

Even when $t'\neq0$, the frequency dependence of the bare structure factor can, in principle, be calculated exactly along the three directions considered previously. However, this time the solution involves finding the roots of a quartic equation, except along the $(q,0)$ direction. We limit ourselves to presenting results for the wave vector $(0,\pi)$ (Appendix C) and for $\mathbf{q}=\mathbf{Q}_{AF}$, which has been extensively studied experimentally.[10(b)] In the latter case we find

$$\chi_0''(\pi,\pi;\omega) = \frac{\Theta(a_-)}{8\pi t}[K(\rho)\Theta(-b_+)+2F(\theta_1,\rho)\Theta(b_+)\theta(a_--\sqrt{b_+})$$

$$-K(\rho)\Theta(-b_-)-2F(\theta_2,\rho)\Theta(b_-)\theta(a_--\sqrt{b_-})] , \tag{22a}$$

where $K(\rho)$ and $F(\theta,\rho)$ are, respectively, the complete and the incomplete elliptic integrals of the first kind. [See Eq. (A23).] The various parameters are defined as follows:

$$a_- \equiv 1 - \frac{\omega}{8t}, \quad a_+ \equiv 1 + \frac{\omega}{8t} ,$$

$$b_- \equiv \left[\frac{\omega}{8t}\right]^2 + \frac{\mu}{4t'} - \frac{\omega}{8t'}, \quad b_+ \equiv \left[\frac{\omega}{8t}\right]^2 + \frac{\mu}{4t'} + \frac{\omega}{8t'} ,$$

(22b)

$$\rho \equiv \sqrt{a_+ a_-} ,$$

$$\theta_1 \equiv \sin^{-1}\left[\frac{a_--\sqrt{b_+}}{a_-(a_+-\sqrt{b_+})}\right]^{1/2} ,$$

(22c)

$$\theta_2 \equiv \sin^{-1}\left[\frac{a_--\sqrt{b_-}}{a_-(a_+-\sqrt{b_-})}\right]^{1/2} .$$

The imaginary part of the bare susceptibility behaves differently according to the nature of the Fermi surface. There are two situations of interest for us, each with three frequency regimes in addition to $\omega>8t$ where $\chi_0''=0$.

For open orbits, $0>\mu>4t'$,

$$\chi_0''(\pi,\pi;\omega) = \frac{1}{8\pi t}[K(\rho)\Theta(\omega-\omega_0)+2F(\theta_1,\rho)\Theta(\omega_0-\omega)$$

$$-2F(\theta_2,\rho)\Theta(\omega_c^--\omega)] \tag{23a}$$

while for closed orbits, $4t'>\mu$.

$$\chi_0''(\pi,\pi;\omega) = \frac{1}{8\pi t}[K(\rho)\Theta(\omega-\omega_0)$$

$$+2F(\theta_1,\rho)\Theta(\omega_0-\omega)]\Theta(\omega-\omega_c^+) \tag{23b}$$

with the critical frequencies defined by

$$\omega_0 \equiv -4\frac{t^2}{t'}\left[1-\left[1-\frac{\mu t'}{t^2}\right]^{1/2}\right] ,$$

$$\omega_c^+ \equiv \frac{-2(\mu-4t')}{(1+2t'/t)} , \tag{24}$$

$$\omega_c^- \equiv \frac{2(\mu-4t')}{(1-2t'/t)} .$$

The two situations are illustrated in Fig. 9. In the case of a Fermi surface with open orbits there is no kinetic gap. When the Fermi surface is closed, however, the gap
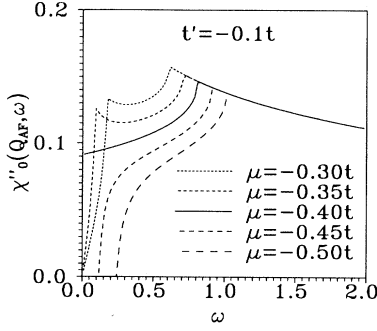
FIG. 9. Frequency dependence of the bare value of χ'' at (π,π) in the next-nearest-neighbor hopping model ($t'=-0.10t$) for various fillings [see Eqs. (22)–(24)]. The limiting case where the Fermi level lies at the Van Hove singularity ($\mu=4t'$) is shown by a solid line. For smaller dopings (larger μ) there is no kinetic gap, while for larger dopings there is a kinetic gap at ω_c^+. The highest energy feature is at $\omega=\omega_0$. The ω_c^- energy is seen in the open-orbit case. [See Eq. (24).]

appears for frequencies less than ω_c^+. Proximity to the Van Hove singularity at $4t'$ can thus introduce a small energy scale. However, unlike the $t'=0$ case where the imaginary part of the susceptibility drops discontinuously to zero at $\omega=2|\mu|$, the imaginary part of the susceptibility vanishes smoothly as ω is decreased towards ω_c^+.

We summarize the important results as follows: (a) The presence of t' has led to a small energy scale (ω_c^- if $\mu>4t'$ and ω_c^+ if $\mu<4t'$). (b) $\chi''(\mathbf{Q}_{AF},\omega)$ has a finite jump as ω vanishes (instead of a kinetic gap) not at half filling, as in the $t'=0$ case, but at a finite doping, corresponding to the Fermi level lying at the Van Hove singularity. (c) The small energy scale leads to MFL ω/T-like scaling of $\chi''(\mathbf{Q}_{AF},\omega)$ for smaller temperatures than in the $t'=0$ case.

IV. STRUCTURE FACTOR AT FINITE U

The generalized RPA for a zero-range potential has the same functional form as the standard RPA. The structure factor in this case is

$$S(\mathbf{q},\omega)=\frac{S_0(\mathbf{q},\omega)}{\{[1-U\chi'(\mathbf{q},\omega)]^2+[U\chi''(\mathbf{q},\omega)]^2\}} \quad . \qquad (25)$$

In a conserving approximation for a zero-range potential, the self-energy just shifts the chemical potential, so it is trivial to take into account. For a quantitative comparison with Monte Carlo data, one needs to use[15] $U_{rn}=U/(1+0.2U)$, instead of the bare value of U, this being understood as coming from summing particle-particle ladders. The self-energy leading to a conserving approximation is then nontrivial,[34] unless a zero-range U_{rn} remains a good approximation for the self-energy calculation as well. In any case, lifetime effects will not be important for the zero-frequency structure factor, as long as this lifetime vanishes at the Fermi surface. If lifetime effects introduce a new energy scale, however, then they will influence the energy dependence of the magnetic structure factor, as shown by Littlewood et al. for the

marginal Fermi-liquid self-energy.[30] For the weak to intermediate-coupling regime, this does not occur in the present microscopic approach.

A. Zero-frequency limit

The zero-frequency low-temperature limit of the magnetic structure factor (25) is

$$S(\mathbf{q})=\frac{S_0(\mathbf{q})}{[1-U_{rn}\chi_0'(\mathbf{q})]^2} \quad . \qquad (26)$$

When t' is equal to zero, the real part of the bare static susceptibility χ_0' has a finite maximum at the pseudonesting wave vector[21] $\mathbf{Q}_n$ and is nonzero in the region where the kinetic gap appears in the imaginary part. Thus, as long as $U_{rn}<1/\chi_0'(\mathbf{Q}_n)$, the vertex corrections represented by the denominator of (17) only enhance the incommensurate peaks that appear as square-root singularities in the bare structure factor in the zero-frequency limit.[35] When $U_{rn}=1/\chi_0'(\mathbf{Q}_n)$, a phase transition to magnetic order occurs.

For $t'<0$ and $\mu>4t'$, a numerical study of the real part of the susceptibility[36] reveals that as long as $t'>-0.25t$, $\chi'(q_x,q_y=\pi,\omega=0)$ has a broad maximum at $\mathbf{Q}_{AF}=(\pi,\pi)$ with a half-width roughly equal to $2\cos^{-1}(-\mu/2t')$. This is illustrated in Fig. 10(a) for various t' at half filling. Results for fixed t' at different fillings are also shown in Fig. 10(b). In the open orbit regime, $\mu>4t'$, illustrated in Fig. 8(a), vertex corrections will enhance those features of the zero-frequency bare structure factor which are close to $\mathbf{Q}_{AF}$. Since most of the interesting features of $S_0(q_x)$ are within this interval, we do not expect any qualitative changes from the $U=0$ limit. However, since the lattice-$2k_F$ anomaly is a singularity only asymptotically close to $T=0$ and $\omega=0$, the maximum will be at $\mathbf{Q}_{AF}$ if $t'>-0.25t$ and if U_{rn} is sufficiently close to the critical interaction U_c. In other words, as long as $t'>-0.25t$, finite negative t' favors a transition to antiferromagnetism instead of an incommensurate spin-density wave, even in cases where the low-frequency maximum of χ_0'' is at an incommensurate position, a rather unintuitive result. At finite frequency and at finite temperatures, the absolute maximum along the (q_x,π) line will be either at the lattice-$2k_F$ anomaly (if μ is close to zero) or at $\mathbf{Q}_{AF}$ (if μ is close to the Van Hove singularity). The transition between the two situations is expected to be strongly temperature and frequency dependent. For the second ($\mu_c^-<\mu<4t'$) and the third regimes ($\mu<\mu_c^-<4t'$), the edge of the kinetic gap in the imaginary part of the susceptibility corresponds to a maximum in its real part. Thus, again, the denominator in (17) enhances the features associated with the kinetic gap. For U sufficiently large there will be a phase transition as in the $t'=0$ case, but we do not consider it any further.

B. Finite-frequency collective modes

At finite frequency, two collective modes appear in the vicinity of the kinetic gap (Fig. 11). For $t'=0$, the first mode has been identified by Bulut and Scalapino.[17,22] In
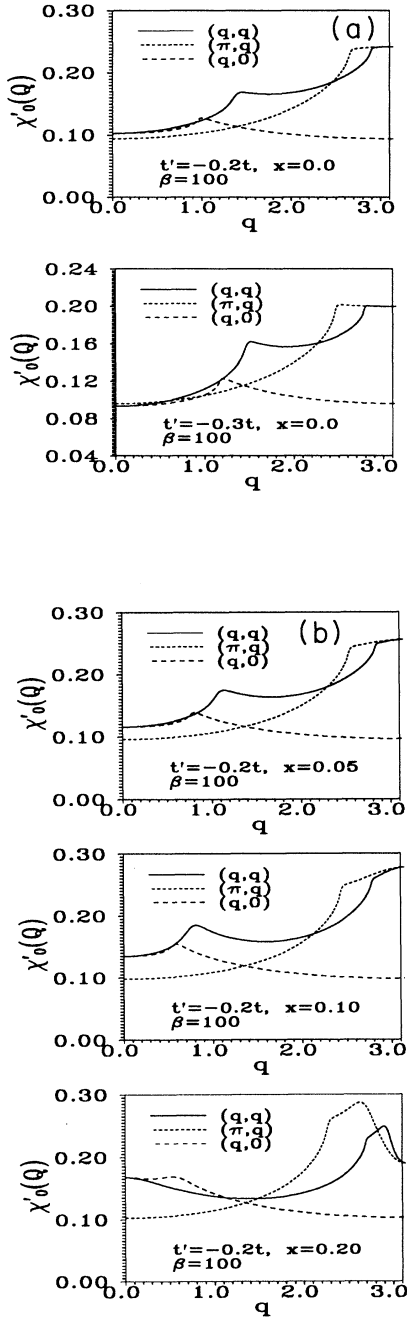
FIG. 10. (a) Real part of the bare, zero-frequency spin susceptibility for a half-filled band in various directions $\mathbf{Q}$ in the Brillouin zone. The directions are distinguished by various symbols as indicated on the figure. It is only for $t' < -0.25t$ that the maximum moves away from (π,π). When this is the case, as in the lower panel, interactions will lead to a magnetic instability at the wave vector which corresponds to the new maximum. (b) The various panels correspond to a fixed value of t' and three different fillings. Since the maximum stays at (π,π) for a range of fillings away from half filling, antiferromagnetism would be stable at finite U_{rn} contrary to the $t'=0$ case where incommensurate magnetism is favored immediately away from half filling.
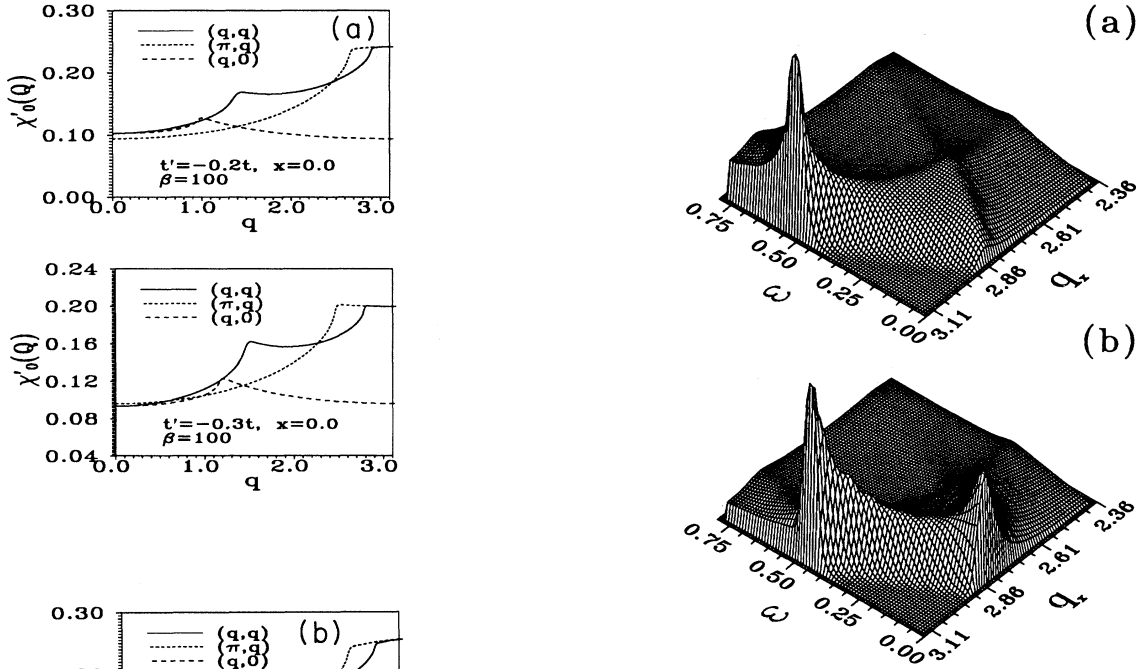

FIG. 11. The imaginary part of the susceptibility at finite U_{rn} for $x = 0.14$, $t' = 0$, (a) $U/U_c = 0.75$, and (b) $U/U_c = 0.975$ for a 4000×4000 lattice (renormalized U values are implied). The overdamped mode softens as U_{rn} approaches the incommensurate spin-density-wave instability at a renormalized value $U_{rn}^c = 2$. The peak in the intensity as a function of wave vector decreases as the frequency ω increases, as long as ω is larger than the resonance frequency.

this case, $\chi_0'(\mathbf{q}=\mathbf{Q}_{AF},\omega)$ diverges logarithmically at the edge of the gap (when $\omega=2|\mu|$) and a finite-frequency mode can then appear inside the gap for arbitrarily small values of U_{rn} since $\chi_0''(\mathbf{q}=\mathbf{Q}_{AF},\omega)$ also vanishes for $\omega < 2|\mu|$. The mode is exponentially close to the particle-hole continuum. It is thus strongly temperature dependent. The mode becomes overdamped as it disperses away from $(\mathbf{Q}_{AF},\omega=2|\mu|)$ into the particle-hole continuum. This mode is closely associated with the presence of the perfect nesting instability at (π,π) for $\mu=0$. In fact, it can be shown that such an undamped mode should be present for any band structure which has a perfect nesting instability at $\mathbf{q}=\mathbf{Q}_n^0$ and $\mu=\mu_0$ (i.e., $\varepsilon_{\mathbf{k}+\mathbf{Q}_n^0}+\varepsilon_{\mathbf{k}}=2\mu_0\forall\mathbf{k}$). Indeed, at μ different from μ_0 and such that there is a kinetic gap, the nesting leads to an edge in $\chi''(\mathbf{q}=\mathbf{Q}_n^0, \omega=2|\mu-\mu_0|)$ which, through the Kramers-Kronig relation, manifests itself as a logarithmic divergence in the real part and hence leads to the collective mode. For $-0.5t < t' < 0$, the mode appears only under very special conditions because there is never perfect nesting. In the case of open orbits, the sharp increase of $\chi_0''(\mathbf{Q}_{AF},\omega)$ at ω_c^- also correspond to a large χ_0' but not to a divergence. For sufficiently strong U there will thus be a large increase at that frequency of the interacting χ''. For a Fermi surface with closed orbits $(\mu < 4t')$, the absence of a discontinuity for

$\chi_0''(\mathbf{q}=\mathbf{Q}_{AF},\omega=\omega_c^+)$ at $T=0$ precludes a singular behavior for $\chi_0'(\mathbf{q}=\mathbf{Q}_{AF},\omega)$ at the edge of the kinetic gap. The singularity is replaced by a finite maximum. Thus, because second-neighbor hopping removes perfect nesting, the mode remains overdamped as long as $\chi_0'(\mathbf{q}=\mathbf{Q}_{AF},\omega=\omega_c^+)$ is less than its zero-frequency maximum. The mode may reappear without damping for small values of t', but only for values of U_{rn} above $U_c=1/\chi_0'(\mathbf{q}=\mathbf{Q}_{AF},\omega=\omega_c^+)$.

The second mode is the spin-density-wave equivalent of paramagnons. It appears as a maximum in the response at finite frequency and wave vector along a feature of the bare response. This maximum is still present for finite t'. As U_{rn} is increased from zero, the maximum softens towards the pseudonesting wave vector as the spin-density-wave instability is approached. The key point here is that close to the phase boundary, the overdamped collective mode introduces a new small energy scale. While the bare magnetic structure factor $S(\mathbf{q})$ increases in frequency, the mode leads to a dressed $S(\mathbf{q})$ which decreases in frequency for a while beyond the maximum. A calculation which includes the fluctuations which destroy long-range order at finite temperature in two dimensions[14,23,24] might lead this energy scale to remain small but finite whenever U_{rn} is larger than the mean-field critical U_{rn}.

V. THEORY AND EXPERIMENT (REF. 37)

A. Position of the incommensurate peaks

Experimentally, the maxima in the neutron-scattering cross section are displaced by $\delta(\pm\pi,0)$ and $\delta(0,\pm\pi)$ from (π,π). Cheong et al.[7] found in $La_{2-x}Sr_xCuO_4$ a value of δ equal to 0.25 ± 0.01 for $x=0.14$ and of 0.14 ± 0.02 for $x=0.075$. In the case of nearest-neighbor hopping only, the position of the peaks is determined by the bare chemical potential at the corresponding concentration:[37]

$$[q_x^0=\pm2\cos^{-1}(-\mu/2t),q_y=\pi]$$

and

$$[q_x^0=\pi,q_y=\pm2\cos^{-1}(-\mu/2t)] \ .$$

Assuming that the concentration x is equal to the doping of the copper-oxygen planes, the above equation predicts a displacement δ of 0.087 for $x=0.14$ and of 0.038 for $x=0.075$. These values are much smaller than allowed by the experimental data. Assuming that the real doping is smaller than x gives corrections in the wrong direction and it does not appear chemically reasonable to assume that the doping is larger than x, unless strong oxygen overdoping occurs. Another discrepancy in comparing theory with experiment is that the observed peaks appear much smoother than predicted. Convolution of the theory with the experimental resolution[30] helps to solve both of these problems. Indeed, because of the proximity of the peaks at $q_x=\pi-\delta\pi$ and $q_x=\pi+\delta\pi$, and because of their strong asymmetry at low temperatures, the measured positions of the peaks may be shifted appreciably from their real positions by experimental resolution.[9] Realistic values of the experimental resolution, however,

do not produce a sufficiently large displacement to accommodate the data. The theoretical value of the shift is still smaller by a factor of about 2.

Next-nearest-neighbor hopping can appreciably shift the position of the incommensurate peaks from their position when $t'=0$, especially close to half filling. Various cases are illustrated in Fig. 12. Consider any of the finite t' curves. The cases with closed orbit but no observable change in curvature are on the right of this plot: There is a single peak and it is not shifted much from its $t'=0$ value. In the regime with closed orbits but curvature changes, there are two peaks $[\mu>\mu_c^-$, Eq. (20)]. The one closest to $\delta=0$ is the largest one, and it is not shifted very much from the $t'=0$ case. When the orbits open $(\mu>4t')$, at smaller doping, one of the peaks stays at $\delta=0$. But as the doping is decreased even more, one moves away from the Von Hove singularity and it is only the peak at large δ which survives.

The case of closed orbits with a single peak is not different enough from the $t'=0$ case to explain the experimental data.[6] To try a fit of the data with a rigid-band model, let us then consider the $x=0.075$ compound in the case when orbits are open. Note that in the open-orbit regime, the repulsion U tends to increase all features uniformly between the incommensurate peak and (π,π) because the real part of the susceptibility is quite flat in this wave-vector range, as seen from Fig. 10. It is only very close to the instability that the antiferromagnetic region becomes enhanced. It thus suffices to consider the noninteracting case. The dotted line in Fig. 13(a) shows for $x=0.075$ that $\delta\approx0.18$ for $t'=-0.16t$, a value of δ slightly larger than the required $\delta\approx0.14$. Since the lattice-$2k_F$ anomaly is holelike, convolution of the experimental resolution will this time move the peak towards (π,π) an effect which tends to make the peak position agree with experiment. However, we see that the rigid-band model fails when we plot the $x=0.14$ case (solid line) since then the maximum is near (π,π) because of the proximity to the Van Hove singularity. If instead we choose $t'=-0.25t$ to make the position of the peak for the latter compound $[\delta\approx0.29$ from the solid line in Fig. 13(b)] agree with experiment after convolution with the
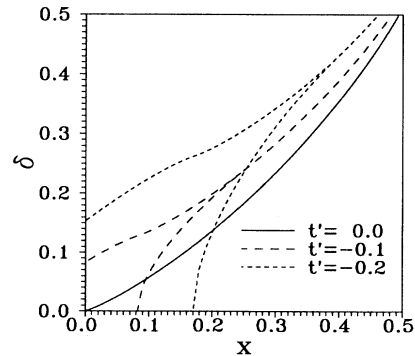

FIG. 12. Peak displacement δ vs dopant concentration x (decreasing μ) for three values of t' (0, -0.1, and -0.2 in units $t=1$) at low temperatures and low frequencies $(T,\omega\ll2|\mu|)$, as predicted by GRPA with renormalized U.

0.015

x=0.14
x=0.075   (a)

ω=0.0025t
t'=−0.16t
β=400

$\chi''(Q,\omega,T)$

0.010

0.005

0.000

2.2   2.4   2.6   2.8   3.0

(q,π)

0.0016

x=0.14   (b)
x=0.075

ω=0.0025t
t'=−0.25t
β=400

$\chi''(Q,\omega,T)$

0.0012

0.0008
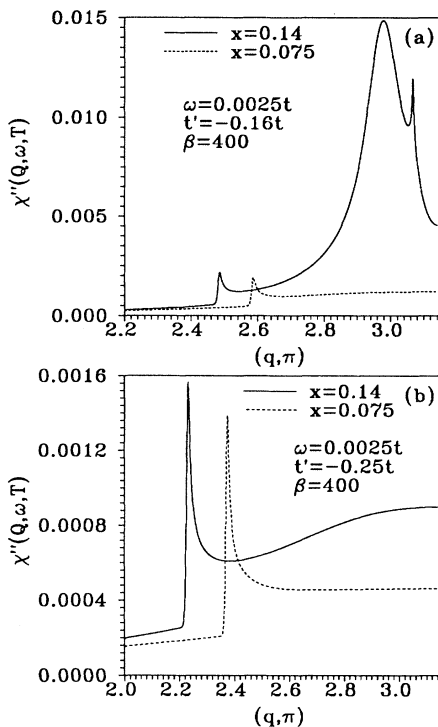
0.0004

0.0000

2.0   2.2   2.4   2.6   2.8   3.0

(q,π)

FIG. 13. Imaginary part of the bare value of the spin suscep-
tibility for open-orbit cases. (a) The dotted line, corresponding
to a concentration $x = 0.075$, has a peak at the experimentally
observed position but for the same value of t' the $x = 0.14$ com-
pound (solid line) has a peak at the wrong position. (b) This
time the peak for the $x = 0.14$ compound (solid line) is at the
correct position, but not that for $x = 0.075$ (dotted line).

experimental resolution, we see that this time it is the
$x = 0.075$ compound whose peak position [$\delta \approx 0.24$ from
the dotted line in Fig. 13(b)] is too far from (π, π) to be
explained by experimental resolution. Assuming a
doping-independent value of t' then (rigid-band model), it
does not appear possible to shift the peaks to their
correct position for both of the experimentally studied
dopings. For a given value of t', however, note that in
the open-orbit regime and at the frequencies of interest
experimentally, the intensity at (π, π) is roughly half the
intensity at the peak position, as observed experimentally.

B. Energy scale

When $t' = 0$, as discussed earlier, the energy scale of
the incommensurate antiferromagnetic spin fluctuations
in the bare structure factor is set by the value of the bare
chemical potential (which measures the difference be-
tween the Fermi energy at finite doping and at half
filling). For temperatures higher than $2|\mu|$, the incom-
mensurate peaks move to (π, π) and nested Fermi-liquid
theory[20] may describe the behavior of the structure fac-
tor.[38] As shown in Fig. 1, experimentally the intensity of
the incommensurate spin fluctuations decreases by about
a factor of 2 for energies (or temperatures) of the order of
150 K for hole doping of 0.14, with respect to the intensi-

ty at (π, π). Since the bare chemical potential is $-0.12t$
for hole doping of 0.07 and $-0.27t$ for hole doping of
0.14, this suggests, for $t \approx 5000$ K, that the energy scale
coming from $t' = 0$ band-structure effects only is 5–10
times too large.

It was shown in Sec. III B that second-neighbor hop-
ping t' can add another small energy scale
$\omega_c^{\pm} = \mp 2(\mu - 4t')/(1 \pm 2t'/t)$, associated with the Van
Hove singularity. On that scale, instead of $2|\mu|$, the in-
commensurate peaks would disappear and scaling similar
to ω/T would be recovered. If t' is chosen to reproduce
as much as possible the peak position of the $x = 0.14$
sample, then ω_c^- is indeed small. However, we just saw
that the same value of t' would predict that the peak is in
the wrong position for the compound with smaller hole
doping, $x = 0.075$. If we insist in keeping the same value
of t', corresponding to open orbits, then the energy scale
should be *larger* for the $x = 0.075$ compound than for the
$x = 0.14$ compound.

We can also take a different point of view, arguing that
the small energy scale must be a fundamental manifesta-
tion of the proximity to a magnetic instability while the
peak positions are a trivial band-structure effect which we
should not worry about. As we have seen in Sec. IV B,
the overdamped mode which becomes soft at the incom-
mensurate transition does provide a mechanism to obtain
a small energy scale in the paramagnetic phase.[39] It can
be objected that one would need again to fine tune the
repulsion, for each value of x, so that the system is close
to the magnetic instability. However, it is likely, but still
unproven, that this small energy scale is present for a
wide range of dopings and interactions when one adds the
long-wavelength fluctuations which remove the finite-
temperature mean-field transition in two dimen-
sions.[14,23,24] Preliminary experimental results[40] seem to
indicate an increase in the intensity of the neutron
scattering for smaller doping. This would be consistent
with the increase in intensity which occurs as the over-
damped mode softens. This is seen in Fig. 11 as a func-
tion of U_{rn} but similar behavior occurs as a function of
doping. Clearly, however, if one remains strictly within
our approach, one needs to be unrealistically close to the
instability to see the decrease in frequency of the magnet-
ic structure factor.

C. Suggestions for further experiments

Within the MFL approach, it is argued that one is far
from any magnetic instability and that the peaks seen in
neutron scattering are purely band-structure effects with
large self-energy corrections (which vanish in the limit of
zero frequency). If this is the case, a number of struc-
tures should be observable experimentally. We suggest to
scan both the $(q, 0)$ and the (q, q) directions. First of all,
let us recall why other incommensurate features away
from (π, π) should appear along these directions if we are
far from a magnetic instability. (a) Incommensurate
features away from (π, π) (see Fig. 5) are as generic on
the square lattice as those already studied experimentally
near (π, π). In particular, we have verified that these
lattice-$2k_F$ anomalies are still present in a three-band
model.[23] (See also Appendix B.) (b) It is only the vertex

corrections (proximity to the instability) which make these peaks away from (π,π) smaller than those near the antiferromagnetic wave vector. As seen in Fig. 5(c), the low-energy scale appearing in the experiments can be explained by the softening of the overdamped mode only if the lattice-$2k_F$ anomaly near zero wave vector is very small.

What can be learned from the lattice-$2k_F$ anomalies along $(q,0)$ and (q,q)? In compounds where incommensurate peaks are observed near (π,π) with little intensity at (π,π), the Fermi surface should be away from the Van Hove singularity and there should be an incommensurate peak in the $(q,0)$ direction if the system is far from a magnetic instability. However, we have encountered a case in the three-band model[23] where the incommensurate peak in the $(q,0)$ direction blends into the peak at the origin even if there are no interactions and there are incommensurate peaks in the vicinity of (π,π). That is why it is important to look in the (q,q) direction as well. In the lightly doped systems the open orbits suggested by the positive Hall coefficient should have a clear signature in the existence of two incommensurate peaks along this direction, as seen in Fig. 19(a) (Appendix B).

Finally, we suggest that neutron-scattering studies at even higher hole doping would be of interest. In particular, if the Hall coefficient becomes negative in $La_{2-x}Sr_xCuO_4$ at a concentration x_H because the Fermi surface closes, then in the concentration range before x_H, the scattering maximum has to go back to the (π,π) point.

VI. CONCLUSIONS

The one-band Hubbard model with second-neighbor hopping t', and U in the intermediate-coupling regime, does explain qualitatively the behavior of the incommensurate spin fluctuations[6,7] in the normal phase of $La_{2-x}Sr_xCuO_4$, in particular the symmetry of the observed maxima in the scattering intensity, and their shift from the simple $t'=0$ case. However, within a rigid-band model where t-t'-U are independent of doping and the concentration x is identified with doping, one cannot account quantitatively for the experimental results since the correct peak positions cannot be obtained for both of the experimentally studied compounds. This lack of detailed agreement may not be too disturbing, however, since we have seen that in two dimension the position of the peaks comes from lattice-$2k_F$ anomalies and is very sensitive to details of the Fermi surface geometry; and even the Fermi surface of the simplest three-band model cannot be described in detail by a single-band model with first- and second-neighbor hopping. Evidently, one must also leave open the possibility of either a failure of the rigid-band model, or the necessity to use strong-coupling approaches.[3–5] Since t' is already a small number, it is not unlikely that the effective Hamiltonian has a value of t' which does depend on doping. In fact, to obtain the correct peak positions, t' would need to become more negative with hole doping. Assuming that the antiferromagnetic transition is most sensitive to the two-dimensional spin susceptibility, the fact that antiferromagnetism disappears with increased doping also suggests that t' becomes more negative with hole doping. (See Fig. 10 to determine the critical U_m as a function of doping.) Slave-boson approaches[3–5] also predict that $|t'|$ must increase with doping in the strong-coupling limit.

More importantly, the second disagreement with experiment is in the existence of a small energy scale, of order 150 K. We have seen that a small energy scale, ω_c^+ or ω_c^- in Eq. (24), can be introduced by second-neighbor hopping in a manner consistent with the displacement of the peaks from the $t'=0$ position. In fact, in several papers[3–5] this is effectively taken as the source of the experimentally observed small energy scale. An alternate explanation of the small energy scale is the occurrence of an overdamped collective mode which softens near the incommensurate magnetic instability. However, as seems to be the case also in previously published interpretations of NMR experiments,[7] one needs to be extremely close to the instability to obtain the correct magnitude of the energy scale. It is still an open question whether the inclusion of fluctuations which destroy long-range order at finite temperature in two dimensions would lead this energy scale to remain small but finite for a wide range of dopings and interactions.

While our approach should be valid up to intermediate coupling, as justified from previous work, its strict applicability would require working far from all the mean-field instabilities, namely, at bare values of U of order $3t$ or less when $t'=-0.2t$. Suggested values of U for high-temperature superconductors are usually in the range $6t-10t$. What happens to the peak position in this strong-coupling limit may be suggested by the recent work of Singh and Glenister.[28] What remains of the overdamped mode in this limit, as well as how critical long-wavelength fluctuations affect the frequency dependence in general, are still open questions. These questions may ultimately need to be answered to completely explain future neutron-scattering experiments or to find a microscopic foundation for the spin-fluctuation kernels entering recent theories of high-temperature superconductors.[41]

Finally, we have pointed out[23] that neutron-scattering experiments could settle the important question of the proximity to a magnetic instability, as raised in particular in the MFL approach.[30] It would suffice to measure the relative size of the incommensurate lattice-$2k_F$ anomalies near zero and near Q_{AF} along both the $(q,0)$ and the (q,q) directions. (See Figs. 5, 18, 19.) These features should be of comparable intensity unless one is extremely close to the transition. If one is indeed far from a magnetic transition, magnetic neutron scattering can provide a detailed spectroscopy of the two-dimensional Fermi surface. In particular, scattering in the diagonal direction (Appendix B) contains characteristic signatures of holelike Fermi surfaces or of changes in curvature induced by second-neighbor hopping (t'). We also gave predictions for larger hole dopings.

APPENDIX A: IMAGINARY PART OF THE LINDHARD FUNCTION ON THE SQUARE LATTICE

Although the two-dimensional $2k_F$ anomalies of the imaginary part of the Lindhard function have already been discussed in Sec. II, we first quote the result for ellipsoidally shaped Fermi surfaces in arbitrary dimension to contrast the two-dimensional result with one and three dimensions. We then give the exact zero-temperature result for tight-binding electrons on the one-dimensional chain and the two-dimensional square lattices, concluding with a finite-temperature result valid near the antiferromagnetic point.

1. Electrons with ellipsoidal Fermi surfaces

We define the imaginary part of the Lindhard function $\chi''(\mathbf{q},\omega)$ in d-dimensional space by

$$\chi_0''(\mathbf{q},\omega)=\frac{\pi}{2(2\pi)^d}\int_{-\infty}^{\infty}dk_1\cdots\int_{-\infty}^{\infty}dk_d\,\delta[\omega-\epsilon(\mathbf{k}+\mathbf{q})+\epsilon(\mathbf{k})]\{f[\epsilon(\mathbf{k})-\mu]-f[\epsilon(\mathbf{k}+\mathbf{q})-\mu]\}\;, \tag{A1}$$

where $\epsilon(\mathbf{k})$ is the energy dispersion, μ is the chemical potential, and $f(x)$ is the Fermi function. One can explicitly integrate the above expression at zero temperature for the hyperellipsoidal energy dispersion relation

$$\epsilon(\mathbf{k})=\sum_{i=1}^{d}\frac{k_i^2}{m_i^2}\;, \tag{A2}$$

obtaining the following simple generalization of the result of Ref. 42:

$$\chi_0''(\mathbf{q},\omega)=\frac{\prod_{i=1}^{d}m_i}{2^{d+2}\pi^{(d-1)/2}\Gamma[(d+1)/2]\sqrt{\epsilon(\mathbf{q})}}\left[\Theta\left[\mu-\frac{[\omega-\epsilon(\mathbf{q})]^2}{4\epsilon(\mathbf{q})}\right]\left[\mu-\frac{[\omega-\epsilon(\mathbf{q})]^2}{4\epsilon(\mathbf{q})}\right]^{(d-1)/2}\right.$$
$$\left.-\Theta\left[\mu-\frac{[\omega+\epsilon(\mathbf{q})]^2}{4\epsilon(\mathbf{q})}\right]\left[\mu-\frac{[\omega+\epsilon(\mathbf{q})]^2}{4\epsilon(\mathbf{q})}\right]^{(d-1)/2}\right]\;. \tag{A3}$$

The real part of the spin susceptibility $\chi''(\mathbf{q},\omega)$ is found using the Kramers-Kronig relation. One obtains

$$\chi_0'(\mathbf{q},\omega)=II(\mathbf{q},\omega)+II(\mathbf{q},-\omega)\;, \tag{A4}$$

where

$$II(\mathbf{q},\omega)=\frac{\mu^{d/2}\prod_{i=1}^{d}m_i}{8\pi^{(d+1)/2}\Gamma[(d+1)/2]}\left[\left[\frac{4\epsilon(\mathbf{q})\mu-[\omega-\epsilon(\mathbf{q})]^2}{4\epsilon(\mathbf{q})\mu}\right]^k\mathcal{A}\right.$$
$$\left.+\frac{\epsilon(\mathbf{q})-\omega}{4\epsilon(\mathbf{q})\mu}\sum_{v=1}^{k}\left[\frac{4\epsilon(\mathbf{q})\mu-[\omega-\epsilon(\mathbf{q})]^2}{16\epsilon(\mathbf{q})\mu}\right]^{v-1}B\left[\frac{d+1-2v}{2},\frac{d+1-2v}{2}\right]\right]\;, \tag{A5}$$

with the value of k and $\mathcal{A}$ depending on whether the dimension is odd or even:

$$\mathcal{A}=\begin{cases}\dfrac{\pi[\epsilon(\mathbf{q})-\omega]}{4\epsilon(\mathbf{q})\mu}\left[1-\Theta\left[1-\dfrac{4\epsilon(\mathbf{q})\mu}{[\epsilon(\mathbf{q})-\omega]^2}\right]\left[1-\dfrac{4\epsilon(\mathbf{q})\mu}{[\epsilon(\mathbf{q})-\omega]^2}\right]^{1/2}\right] & (\text{if } d=2k+2)\;,\\[6mm]\dfrac{1}{2\sqrt{\epsilon(\mathbf{q})\mu}}\ln\left|\dfrac{\epsilon(\mathbf{q})-\omega+2\sqrt{\epsilon(\mathbf{q})\mu}}{\epsilon(\mathbf{q})-\omega-2\sqrt{\epsilon(\mathbf{q})\mu}}\right| & (\text{if } d=2k+1)\;,\end{cases} \tag{A6}$$

$$B(x,y)=\frac{\Gamma(x)\Gamma(y)}{\Gamma(x+y)}\;. \tag{A7}$$

This form differs from that in Ref. 42. Note that when using the above formula for $d = 1$ and 2 one should take $k = 0$ which means that only the $\mathcal{A}$ term survives in the large square brackets of Eq. (A6).

A few plots of $\chi''(q,\omega)$ should now show that spin fluctuations are strongly dependent on the dimensionality for the free fermions: Higher dimension tends to diminish the sharp features in the spin fluctuations around $2k_F$ ($2k_F$ anomalies). While there are sharp peaks around $2k_F$ in the low-frequency spin fluctuations of both one- and two-dimensional noninteracting fermions, this is not true in three and more dimensions where interactions more than the Fermi surface will determine the position of peaks in the neutron-scattering cross sections. (In the next section we will show this is true for tight-binding electrons as well.)

In the following plots we take $m_i \equiv 1$ without loss of generality. ω is measured in units of the Fermi energy. In Fig. 14 the one-dimensional $\chi''(q,\omega)$ is plotted as a function of q for several frequencies. It is seen that when ω is small $\chi''(q,\omega)$ has sharp features in two separate regions of q space, one near the origin and the other near $2k_F$. As ω increases, the peak around $2k_F$ broadens faster than the peak close to (0,0). If ω is increased even further the peak near the origin disappears, leaving only one (0,0) peak tailing away at $2k_F$.

In Fig. 15, the top panel shows $\chi''(q,\omega)$ for two-dimensional free fermions. There are still two peaks at small frequencies, one near the origin and the other near $2k_F$. The latter is considerably weakened in contrast with one dimension. As in Sec. II, one can show for small ω that $\chi''(q,\omega) \propto \sqrt{\omega}$ at the peak positions. Therefore, any linear expansion of $\chi''(q,\omega)$ for small ω fails close to these two peaks. It is worthwhile to emphasize again that the peak around $2k_F$ exists in two dimensions even without nesting. Similar to the one-dimensional case, as ω increases the peak near the origin disappears leaving only a single broad feature. The bottom panel of Fig. 15 shows $\chi''(q,\omega)$ for three-dimensional free fermions. In contrast with the other two cases, there is no sharp peak around $2k_F$ except a "kink" for small frequencies. At larger frequency the behavior is similar to the two-dimensional case.
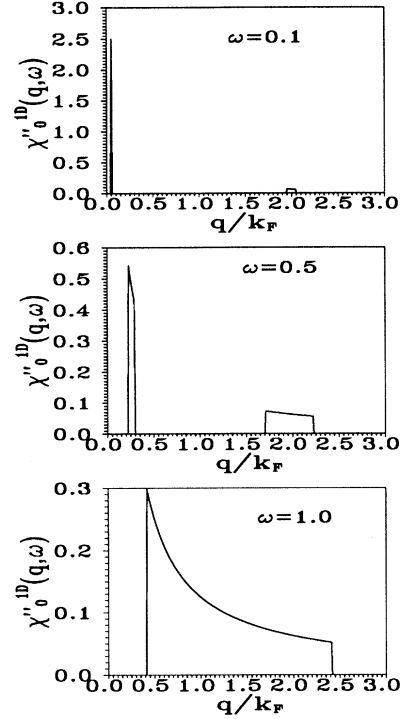

FIG. 14. Imaginary part χ'' as a function of q/k_F for several frequencies. The electrons are free in a one-dimensional continuum. ω is measured in units of the chemical potential k_F^2. The sharp features of the top graph broaden when ω increases, until a single feature is left.

2. Tight-binding electrons

First in the one-dimensional tight-binding case

$$\epsilon_{1d}(k) = -2t\cos(k) , \tag{A8}$$

one can find the exact expression for the imaginary part of spin susceptibility in the zero-temperature limit:

$$\chi_0''^{1D} = \frac{\Theta\{[4t\sin(q/2)]^2 - \omega^2\}}{4\sqrt{[4t\sin(q/2)]^2 - \omega^2}} \left[\Theta\left[\mu + \frac{\omega}{2} + \frac{1}{2}\cot\frac{q}{2}\sqrt{[4t\sin(q/2)]^2 - \omega^2}\right] + \Theta\left[\mu + \frac{\omega}{2} - \frac{1}{2}\cot\frac{q}{2}\sqrt{[4t\sin(q/2)]^2 - \omega^2}\right] \right.$$

$$- \Theta\left[\mu - \frac{\omega}{2} + \frac{1}{2}\cot\frac{q}{2}\sqrt{[4t\sin(q/2)]^2 - \omega^2}\right]$$

$$\left. - \Theta\left[\mu - \frac{\omega}{2} - \frac{1}{2}\cot\frac{q}{2}\sqrt{[4t\sin(q/2)]^2 - \omega^2}\right] \right] . \tag{A9}$$

Figure 16 shows $\chi''(q,\omega)$ as a function of q for several frequencies when the doping is $x = 0.14$. The behavior is similar to that of fermions in the continuum. It is only at high frequency where one peak extends beyond the wave vector $q = \pi$ that a new small-step feature appears.

More interestingly, for the two-dimensional tight-binding band

$$\epsilon_{2D}(\mathbf{k}) = -2t\cos(k_x) - 2t\cos(k_y) , \tag{A10}$$

one can also obtain exactly, in the zero-temperature limit,

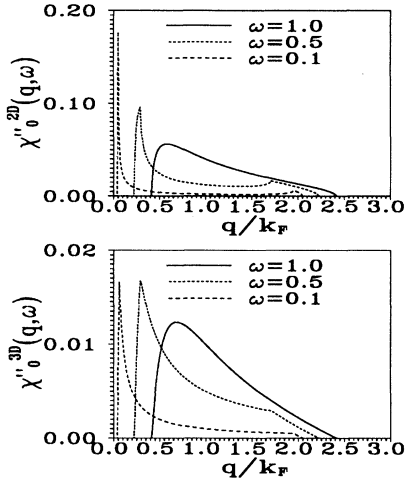FIG. 15. χ_0'' is plotted as in Fig. 14 but for two-dimensional free electrons. The peaks are less sharp than in the one-dimensional case. The bottom panel shows the three-dimensional result. Only a kink is left at $2k_F$ for small frequencies.

the imaginary part of spin susceptibility $\chi''(\mathbf{q},\omega)$. The solution is expressed in terms of elliptic integrals, but for a general direction of $\mathbf{q}=(q_x,q_y)$ one needs to solve a fourth-order algebraic equation. However, it turns out one can get a relatively simple expression in the high-
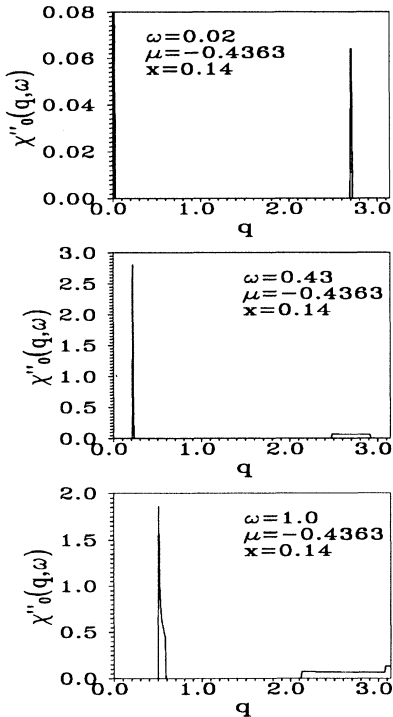
FIG. 16. Exact result for the imaginary part of the spin susceptibility in the one-dimensional nearest-neighbor one-band Hubbard model. The three panels show three different frequencies. New features appear as the frequency increases. (ω and μ are in units of $t=1$.)

symmetry directions $\mathbf{q}=(q_x,0)$, (q_x,π), and (q,q).

Using the usual mappings we can restrict ourselves to the $\mu \le 0$ case, without loss of generality. Let us define

$$\epsilon(\mathbf{k}) \equiv -2t(\cos k_x + \cos k_y) \;, \tag{A11}$$

$$I(\mathbf{q},\omega) \equiv \frac{1}{8\pi} \int_0^{2\pi} dk_x \int_0^{2\pi} dk_y \delta \left[\omega - \epsilon \left[\mathbf{k}+\frac{\mathbf{q}}{2} \right] \right.$$

$$\left. + \epsilon \left[\mathbf{k}-\frac{\mathbf{q}}{2} \right] \right]$$

$$\times \Theta \left[\mu - \epsilon \left[\mathbf{k}-\frac{\mathbf{q}}{2} \right] \right] \;, \tag{A12}$$

then

$$\chi_0''(\mathbf{q},\omega) \equiv I(\mathbf{q},\omega) - I(\mathbf{q},--\omega) \;. \tag{A13}$$

From now on, we work in units where $t=1$. Note also that the results for $I(\mathbf{q},\omega)$ and for $I(\mathbf{q},-\omega)$ are quoted separately because, in general, the analytic continuation of the function $I(\mathbf{q},\omega)$ from ω to $-\omega$ is not trivial. For this reason, we will always assume $\omega \ge 0$ below.

First in the $\mathbf{q}=(q_x,0)$ direction, let us introduce the function

$$\mathrm{acos}(x) = \begin{cases} 0 & \text{if } x>1 \;, \\ \arccos(x) & \text{if } -1\le x \le 1 \;, \\ \pi & \text{if } x<-1 \;, \end{cases} \tag{A14}$$

$$\alpha(q_x,\pm\omega) = \mathrm{acos} \left[\frac{1}{4}\cot\frac{q_x}{2}\sqrt{[4\sin(q_x/2)]^2-\omega^2} \right.$$

$$\left. -\frac{2\mu\pm\omega}{4} \right] \;, \tag{A15}$$

$$I_1(q_x,\pm\omega) = \frac{\Theta\{[4\sin(q_x/2)]^2-\omega^2\}}{4\pi\sqrt{[4\sin(q_x/2)]^2-\omega^2}}$$

$$\times [\alpha(q_x,\pm\omega)+\alpha(-q_x,\pm\omega)] \;. \tag{A16}$$

Then we have

$$\chi_0''^{2D}[(q_x,0),\omega] = I_1(q_x,\omega) - I_1(q_x,-\omega) \;. \tag{A17}$$

In the diagonal direction $\mathbf{q}=(q,q)$ we must consider separately the cases $\omega<2|\mu|$ and $\omega\ge 2|\mu|$. For the $\omega<2|\mu|$, let us define the angles γ, $\beta^\pm$, $\phi^\pm$, all contained in the $[0,\pi/2]$ interval:

$$\sin\gamma = \frac{\omega}{8\sin(q/2)} \;, \tag{A18}$$

$$\tan\beta^\pm = \frac{\omega\cot(q/2)}{2|\mu|\mp\omega} \;, \tag{A19}$$

$$\sin\phi^\pm = \frac{\cos\beta^\pm}{\cos\gamma} \;. \tag{A20}$$

Then,

$$I_2(q,\pm\omega)=0 \quad \text{for } \beta^\pm \leq \gamma \; , \tag{A21}$$

while for $\beta\pm \geq \gamma$

$$I_2(q,\pm\omega)=\frac{\Theta[8\sin(q/2)-|\omega|]}{16\pi\sin(q/2)}$$
$$\times\left[F\left[\frac{\pi}{2},\cos\gamma\right]-F(\phi^\pm,\cos\gamma)\right] \; , \tag{A22}$$

where

$$F(\phi,k)=\int_0^\phi\frac{d\alpha}{\sqrt{1-k^2\sin^2\alpha}} \tag{A23}$$

is the incomplete elliptic integral of the first kind. For $\omega\geq 2|\mu|$ the expression for $I_2(q,-\omega)$ is unchanged. For $I_2(q,\omega)$ we define another angle β'^+ contained in the $[\pi/2,\pi]$ interval:

$$\beta'^+=\pi+\arctan\left[-\frac{\omega\cot(q/2)}{\omega-2|\mu|}\right] \; . \tag{A24}$$

Then, for $\beta'^+ \geq \pi-\gamma$,

$$I_2(q,\omega)=\frac{\Theta[8\sin(q/2)-\omega]}{8\pi\sin(q/2)}F\left[\frac{\pi}{2},\cos\gamma\right] \; , \tag{A25}$$

and, for $\pi/2\leq\beta'^+ <\pi-\gamma$,

$$I_2(q,\omega)=\frac{\Theta[8\sin(q/2)-\omega]}{16\pi\sin(q/2)}$$
$$\times\left[F\left[\frac{\pi}{2},\cos\gamma\right]+F(\phi'^+,\cos\gamma)\right] \tag{A26}$$

with

$$\phi'^+=\arcsin\left[\frac{\cos(\pi-\beta'^+)}{\cos\gamma}\right] \; . \tag{A27}$$

Finally we have

$$\chi_0''^{2D}[(q,q),\omega]=I_2(q,\omega)-I_2(q,-\omega) \; . \tag{A28}$$

These results in the diagonal direction differ from previously published ones.[25] Comparison with full numerical integration of the original expression confirms our analytical result.

The last direction we are interested in is $q=(q_x,\pi)$. Define

$$\cos\delta^\pm=\frac{2|\mu|\mp\omega}{4\cos(q_x/2)} \tag{A29}$$

with $0\leq\delta^\pm\leq\pi/2$, and

$$d^\pm\equiv\sin\delta^\pm \; , \tag{A30}$$

$$s\equiv\sin(q_x/2) \; , \tag{A31}$$

$$v\equiv\omega/4 \; . \tag{A32}$$

Then for $\omega\leq 2|\mu|$ we have

$$I_3(q_x,\pm\omega)=A\left[F\left[\frac{\pi}{2},\kappa\right]-F(\phi_1^\pm,\kappa)-F(\phi_2^\pm,\kappa)\right]$$
$$\times\Theta[4\cos(q_x/2)-2|\mu|\pm\omega] \tag{A33}$$

with A, κ, $\phi_1^\pm$, and $\phi_2^\pm$ taking the following values in different intervals:
for $1-v>s$:

$$A=(8\pi)^{-1}[(1+s)^2-v^2]^{-1/2} \; ,$$
$$\kappa=16\pi A\sqrt{s} \; ,$$
$$\phi_1^\pm=\arcsin\left[\left[\frac{1-d^\pm}{2}\frac{1+s-v}{1-sd^\pm-v}\right]^{1/2}\right] \; ,$$
$$\phi_2^\pm=\arcsin\left[\left[\frac{1-d^\pm}{2}\frac{1+s+v}{1-sd^\pm+v}\right]^{1/2}\right] \; , \tag{A34}$$

for $sd^\pm<1-v<s$:

$$A=(16\pi)^{-1}s^{-1/2} \; ,$$
$$\kappa=8\pi A\sqrt{(1+s)^2-v^2} \; ,$$
$$\phi_1^\pm=\arcsin\left[\left[\frac{1}{1-d^\pm}\frac{1-sd^\pm-v}{1+s-v}\right]^{1/2}\right] \; ,$$
$$\phi_2^\pm=\arcsin\left[\left[\frac{2s(1-d^\pm)}{(1+s-v)(1-sd^\pm+v)}\right]^{1/2}\right] \; , \tag{A35}$$

for $-sd^\pm<1-v<sd^\pm$:

$$A=(16\pi)^{-1}s^{-1/2} \; ,$$
$$\kappa=8\pi A\sqrt{(1+s)^2-v^2} \; ,$$
$$\phi_1^\pm=0 \; ,$$
$$\phi_2^\pm=\arcsin\left[\left[\frac{2s(1-d^\pm)}{(1+s-v)(1-sd^\pm+v)}\right]^{1/2}\right] \; . \tag{A36}$$

Finally, for $1-v<-sd^\pm$ we have $I_3(q_x,\pm\omega)=0$.

The last case we need to consider in this $q=(q_x,\pi)$ direction is $\omega>2|\mu|$. The expression for $I_3(q_x,-\omega)$ is the same as above but for $I_3(q_x,\omega)$, we need to be more specific. First, notice that δ^+ is in the interval $[\pi/2,\pi]$ when $0<\omega-2|\mu|<4\cos(q_x/2)$ while δ^+ must be taken to equal to π when $\omega-2|\mu|>4\cos(q_x/2)$. Considering $\pi/2\leq\delta^+<\pi$, and the first three intervals, namely, $1-v>s$, $sd^+<1-v<s$, and $-sd^+<1-v<sd^+$, the answers have the same algebraic forms as for $\omega<2|\mu|$ except that ϕ_1^+ and ϕ_2^+ have opposite sign [remember also that $F(-\phi,k)=-F(\phi,k)$]. The fourth of the previous intervals, $1-v<-sd^+$, is split in two now: In $-s<1-v<-sd^+$, the algebraic expression is the same as the last third interval except $\phi_2^+=-\pi/2$; and if $1-v<-s$ we again have $I_2(q_x,\omega)=0$. When δ^+ is equal to π, namely, when $\omega-2|\mu|>4\cos(q_x/2)$, we find that when $1-v>s$, A and κ have the same value as they had for smaller δ^+ while $\phi_1^+=0$ and $\phi_2^+=-\pi/2$. For $-s<1-v<s$, the situation is the same as in the $-s<1-v<-sd^+$ case just discussed for $\pi/2<\delta^+<\pi$.

Lastly, when $1-v < -s$ we have $I_3(q_x,\omega)=0$. Therefore,

$$\chi_0''^{2D}[(q_x,\pi),\omega]=I_3(q_x,\omega)-I_3(q_x,-\omega) .   \qquad (A37)$$

Figure 7 shows $\chi''(\mathbf{q},\omega)$ along these highly symmetric directions for several frequencies when the doping is $x=0.14$. Even for frequency less than twice the chemical potential, extra features due to the geometry of the Fermi surface are shown in Fig. 17 in which the peak near the origin splits into two closely separated ones followed by a broad *umklapp* peak.

Finally let us discuss $\chi''(\mathbf{q},\omega)$ at finite temperature for the two-dimensional tight-binding band. One can have the following form of the imaginary part of spin suscepti-bility:
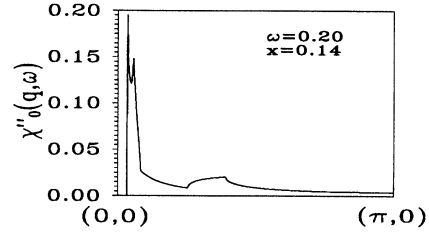

FIG. 17. Effect on $\chi''(\mathbf{q},\omega)$ of Fermi surface geometry at finite frequency. The plot shows the exact two-dimensional tight-binding electron result in the direction $(q_x,0)$. It is seen that the peak near the origin splits into two, and is followed by a broad *umklapp* peak. This figure is an enlargement of part of Fig. 7(b). (ω and μ are in units of $t=1$.)

$$\chi_0''(\mathbf{q},\omega)= \int \frac{d\mathbf{k}}{8\pi} \frac{\sinh(\beta\omega/2)\delta[\omega-4t\sin(q_x/2)\sin k_x-4t\sin(q_y/2)\sin k_y]}{\cosh(\beta\omega/2)+\cosh\{\beta[\mu+2t\cos(q_x/2)\cos k_x+2t\cos(q_y/2)\cos k_y]\}} ,   \qquad (A38)$$

where $\beta=1/T$ and the integration is over the first Brillouin zone. It is interesting to look at the asymptotic form of the above expression around point $\mathbf{q}=(\pi-\tilde{q}_x,\pi-\tilde{q}_y)$ for small $\tilde{q}_x$ and $\tilde{q}_y$ at low frequency ω, we get

$$\chi_0'' \approx \frac{\pi}{16}N\left[\frac{\omega}{2}\right]\sinh\left[\frac{\beta\omega}{2}\right]\left[\frac{1}{\cosh(\beta\omega/2)+\cosh\{\beta[\mu+t(\tilde{q}_x+\tilde{q}_y)]\}} + \frac{1}{\cosh(\beta\omega/2)+\cosh\{\beta[\mu-t(\tilde{q}_x+\tilde{q}_y)]\}}\right.$$

$$\left. + \frac{1}{\cosh(\beta\omega/2)+\cosh\{\beta[\mu+t(\tilde{q}_x-\tilde{q}_y)]\}} + \frac{1}{\cosh(\beta\omega/2)+\cosh\{\beta[\mu-t(\tilde{q}_x-\tilde{q}_y)]\}}\right] .$$

$$\qquad (A39)$$

Here

$$N\left[\frac{\omega}{2}\right]=\frac{1}{t\pi^2}K[\sqrt{1-(\omega/8t)^2}]   \qquad (A40)$$

is the density of states and $K(x)$ is the complete elliptical integral. From the above equation one can easily argue that the maximum value of χ'' near (π,π) in the direction $(\pi-\tilde{q}_x,\pi)$ is twice of that in the direction $(\pi-\tilde{q},\pi-\tilde{q})$ in the limit of low temperature and small frequency. This can be seen clearly from the top graph of Fig. 5. This dis-cussion is different from a previously published result.[43]

APPENDIX B: STRUCTURE FACTOR WITH $t'\ne0$ ALONG (q,q) AND $(q_x,0)$ FOR T AND ω SMALL

Even with $t'\ne0$, interactions will, in general, enhance the spectral features near $(\pi,\pi-\delta)$. Nevertheless, we have shown in Ref. 23 that unless one is very close to a magnetic instability, the features present at $U=0$ will persist at finite U. When $t'\ne0$, the diagonal direction then becomes extremely interesting since it is very sensi-tive to t', showing qualitative differences with the case $t'=0$. These differences would allow one to differentiate, for example, between open- and closed-orbit situations. In this appendix then, we calculate exactly the low-frequency low-temperature limiting form of the structure factor along the two other high-symmetry directions (q,q) and $(q_x,0)$, using Eq. (11).

As usual we do not explicitly write the Heaviside func-tions which lead to a vanishing of the corresponding term whenever the argument of a square root is negative. We first start with the $(q_x,0)$ direction:
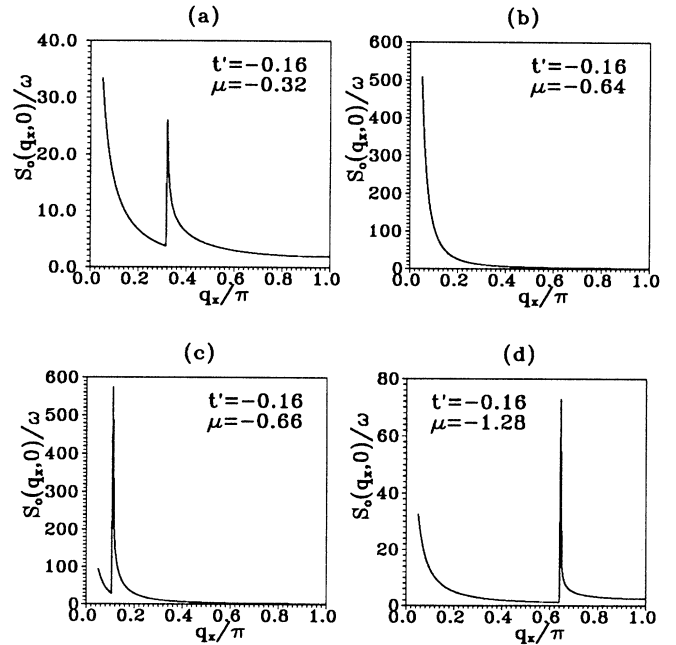

FIG. 18. Wave-vector dependence of the bare structure fac-tor, divided by frequency, at asymptotically low temperature for $t'=-0.16t$ (Appendix B) along the line $(q_x,0)$. The four re-gions correspond to the three Fermi surface shapes discussed in Fig. 2(a), and to the limiting case (b) where the Fermi surface is at the Van Hove singularity. [See Fig. 8 for the corresponding cases in the (q_x,π) direction.]

$$S_0(q_x,0) = \frac{\max(T,\omega)}{8\pi \sin(q_x/2)|t^2-t'\mu|} \left[\frac{t-2t'\cos(q_x/2)}{\sqrt{[4t'\cos(q_x/2)-2t]^2-[\mu-2t\cos(q_x/2)]^2}} \right.$$
$$\left. + \frac{t+2t'\cos(q_x/2)}{\sqrt{[4t'\cos(q_x/2)+2t]^2-[\mu+2t\cos(q_x/2)]^2}} \right].$$

(B1)

The result is illustrated in Fig. 18 for various fillings. The overall shape is qualitatively similar to the $t'=0$ case illustrated in Fig. 5(a) (peak no. 2). The main qualitative difference is in the doping dependence of the position of the *umklapp* peak. This doping dependence, in principle, allows one to bracket the doping at which the Fermi surface just closes. Indeed, when $t'\neq0$, the peak moves towards the origin as we hole dope from half filling until the orbits just close [Fig. 18(b)]. The peak then moves away from the origin as the system is doped further, as in the $t'=0$ case. This is easy to understand from the shape of the Fermi surface illustrated in Fig. 3(a). In the open-orbit case, the peak corresponds to the shortest vector, along the edges of the zone, which links two disconnected sections of the Fermi surface.

The more interesting result is along the diagonal. We obtain $S_0(q,q)=S_0^1(q,q)+S_0^2(q,q)$ with

$$S_0^1(q,q) = \frac{\max(T,\omega)}{32\pi|tt'| \sin(q/2)\sqrt{A_1}}$$
$$\times \left[\frac{1}{|\sqrt{A_1}-\cos(q/2)(t/2t'-2t'/t)|\sqrt{1-[\sqrt{A_1}-(t/2t')\cos(q/2)]^2}} \right.$$
$$\left. + \frac{1}{|\sqrt{A_1}+\cos(q/2)(t/2t'-2t'/t)|\sqrt{1-[\sqrt{A_1}+(t/2t')\cos(q/2)]^2}} \right],$$

(B2)

where

$$A_1 = -\frac{\mu}{4t'} + \sin^2\left[\frac{q}{2}\right] + \frac{t^2}{4t'^2}\cos^2\left[\frac{q}{2}\right],$$

(B3)

$$S_0^2(q,q) = \frac{\max(T,\omega)|8t'\cos(q/2)|\Theta\{[2t'\cos(q/2)]^2-t^2A_2\}}{16\pi\sin(q/2)\sqrt{A_2(1-A_2)}\left|4t'-\frac{t^2}{t'\cos^2(q/2)}\right||[2t'\cos(q/2)]^2-t^2A_2|},$$

(B4)

where

$$A_2 \equiv \frac{4t'\cos^2(q/2)-\mu}{4t'-t^2/t'\cos^2(q/2)}.$$

(B5)

This is illustrated in Fig. 19. In both the open- and closed-orbit cases there is now the possibility of obtaining results which are qualitatively different from the $t'=0$ case. Before we begin a more detailed discussion, let us define four wave-vector components q_0 to q_3 which locate the position of singularities in the various cases:

$$\cos^2\left[\frac{q_0}{2}\right] = \frac{\mu}{4t'},$$
$$\cos\left[\frac{q_1}{2}\right] = \mathrm{sgn}(\mu)\left\{\frac{t}{2t'} + \left[\left[\frac{t}{2t'}\right]^2 - \frac{\mu}{4t'}\right]^{1/2}\right\},$$
$$\cos^2\left[\frac{q_2}{2}\right] = \frac{1-\mu/4t'}{1-(t/2t')^2},$$
$$\cos^2\left[\frac{q_3}{2}\right] = -\frac{1-\mu/4t'}{1-(2t'/t)^2}.$$

(B6)

We start the discussion with the open-orbit case, near half filling. In the hole-doped case, the Fermi surface intersects the 45° line illustrated by the dotted line in Fig.

20, allowing the existence of the two lattice-$2k_F$ vectors shown by arrows. The shortest one is an *umklapp* vector. These two vectors lead to the two well-separated peaks in Fig. 19(a). This should be contrasted with the $t'=0$ case where a single peak appears. The two peaks tail towards large q because of the holelike curvatures of the sections of Fermi surface they join. If the system is sufficiently electron doped, the Fermi surface does not cross the dotted line in Fig. 20, and we recover the case of a single peak (not shown in Fig. 19).

Returning to hole doping, when the Fermi surface just closes, as in Fig. 19(b), the (π,π) vector joins the Van Hove singularity points and, as in the case of the (q_x,π) direction in Fig. 8, the vanishing of the Fermi velocities leads to a huge intensity at (π,π).

When the Fermi surface is closed a bit more by doping, it exhibits changes in curvature. This leads to three possible singular wave vectors, defined by $Q_1=(q_1,q_1)$ to $Q_3=(q_3,q_3)$ above. One of these, while involving no *umklapp* processes, has no free-electron analog. This is the large, almost symmetrical, peak in Fig. 19(c). It comes from the Q_3 vector in Fig. 21. We are in the situation discussed in Eq. (12c) with $R_+=R_-$ and $\psi=\pi/2$, so that the singularity at Q_3 is in $1/\Delta q$ instead of the usual $1/\sqrt{\Delta q}$. Such $1/\Delta q$ singularities occur in the free-electron case only near the origin. This behavior would

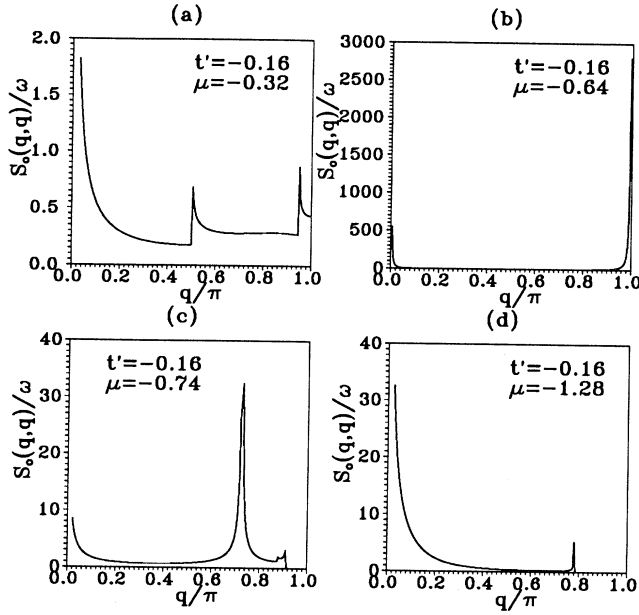PIERRE BÉNARD, LIANG CHEN, AND A.-M. S. TREMBLAY

FIG. 19. Same quantity as in Fig. 18, but along the diagonal direction. The other parameters are identical, except for the case $\mu = -0.66$ ($t \equiv 1$) which has been replaced here by $\mu = -0.74$ to enhance the separation between the Q_1 and Q_2 peaks.

lead to a stronger temperature dependence than for the usual case, but it occurs in a regime where even the $1/\sqrt{\Delta q}$ peaks strongly depend on temperature because of the smallness of ω_c^+. This is illustrated in Fig. 22. Returning to Fig. 19(c), note that, in general, the relative position of the three peaks may change and that in the specific case illustrated, the two peaks nearest (π,π) would, in practice, be impossible to resolve.

The last situation is when the Fermi surface has a single curvature, namely, when $\mu < \mu_c$, with
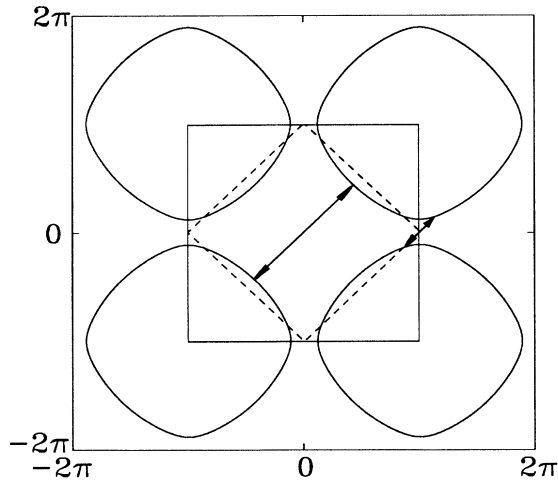

FIG. 20. The two wave vectors corresponding to the two singularities in the open-orbit case in Fig. 19(a).
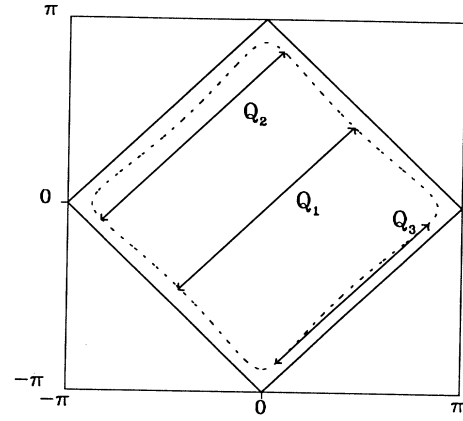

FIG. 21. The three wave vectors corresponding to the three singularities in Fig. 19(c) when orbits are closed and there are changes in the curvatures of the Fermi surface. The Fermi surface is shown as a dashed line. The solid line is a guide to the eye to enhance the curvature of the Fermi surface. The Q_3 wave vector leads to a $1/\Delta q$ singularity. The analytic expressions for the wave vectors are in Appendix B.
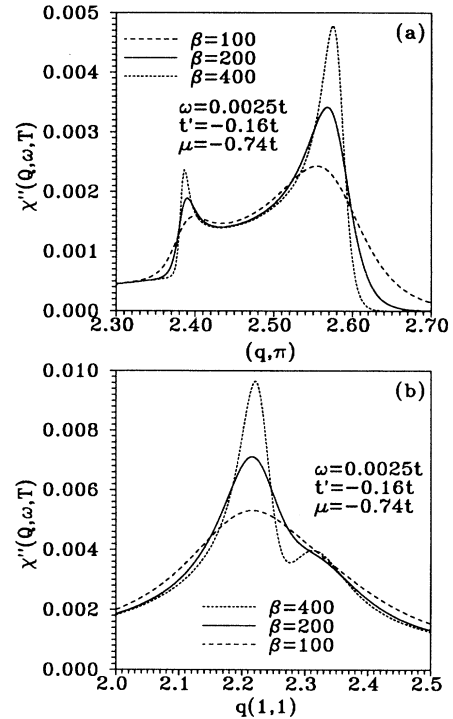

FIG. 22. (a) Temperature dependence along the (q_x,π) direction [see also Fig. 8(c)]. The $1/\sqrt{\Delta q}$ peaks, exceptionally, also have a strong temperature dependence because of the smallness of ω_c^+. (b) Temperature dependence of the $1/\Delta q$ singularity along the diagonal direction at Q_3 when the orbits are just closed [Fig. 19(c)]. As seen in the figure, as long as the frequency is finite, two peaks can be resolved at sufficiently low temperature. The separation between the peaks decreases with frequency. This effect is similar to that seen near the origin in Fig. 17 but the sensitivity to frequency is stronger here.

$$\mu_c \equiv 4t' \left[2 - \left[\frac{2t'}{t} \right]^2 \right] . \tag{B7}$$

In this case, illustrated in Fig. 19(d), a single peak located at $\mathbf{Q}_1$ appears. Note that the diagonal direction is more sensitive to changes in curvature than the (q, π) direction since $\mu_c < \mu_c^-$, where μ_c^- is defined by Eq. (20).

APPENDIX C: ANALYTICAL RESULTS FOR $\chi''[(\mathbf{q}=(0,\pi),\omega]$ WITH FIRST- AND SECOND-NEIGHBOR HOPPING

The result will be written in the form

$$\chi_0''(\mathbf{q},\omega) = I_4(\mathbf{q},\omega) - I_4(\mathbf{q},-\omega) , \tag{C1}$$

where $\mathbf{q} = (0,\pi)$. The result for $I_4(\mathbf{q},-\omega)$ may be obtained from $I_4(\mathbf{q},\omega)$ simply by using

$$\varepsilon_0' \equiv \frac{4t'}{t} \left| \mu - \frac{\omega}{2} \right| \tag{C2}$$

instead of

$$\varepsilon_0 \equiv \frac{4t'}{t} \left| \mu + \frac{\omega}{2} \right| \tag{C3}$$

in locating the various intervals. We identify four regions, which, in turn, are subdivided in several possibilities depending on the value of ε_0.
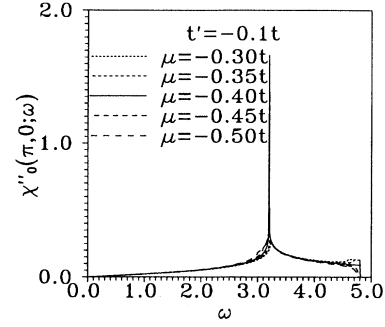
FIG. 23. Exact result for the frequency dependence of the imaginary part of the spin susceptibility χ'' at $\mathbf{q}=(\pi,0)$ for electrons on a lattice, including second-neighbor hopping $t'=-0.1t$ (see Appendix C). The result depends very little on filling. A logarithmic singularity appears at $\omega=4t+8t'$.

First, in the region $4t-\omega < 8t'$, we have

$$I_4(\mathbf{q},\omega) = 0 . \tag{C4}$$

Second, in the region where $8t' < 4t-\omega \le -8t'$ and $4t+\omega \ge -8t'$ we find

$$I_4(\mathbf{q},\omega) = 0 \quad \text{if } \varepsilon_0 > 4t-\omega , \tag{C5a}$$

and, otherwise,

$$I_4(\mathbf{q},\omega) = \frac{1}{2\pi} \frac{1}{2\sqrt{2\omega t'}} F(\theta_1, q_1) ,$$

$$q_1 \equiv \left[\frac{(4t+\omega+8t')(4t-\omega-8t')}{-32\omega t'} \right]^{1/2} ,$$

$$\theta_1 \equiv \begin{cases} \arcsin \left[\dfrac{-16t'}{4t-\omega-8t'} \dfrac{4t-\omega-\varepsilon_0}{-8t'-\varepsilon_0} \right]^{1/2} & \text{if } 8t' < \varepsilon_0 \le 4t-\omega , \\ \pi/2 & \text{if } \varepsilon_0 < 8t' . \end{cases} \tag{C5b}$$

In the last two regions, $I_4(\mathbf{q},\omega) = 0$ when $\varepsilon_0 > -8t'$. The other cases within these two regions must be considered separately. In the third region, delimited by $8t' < 4t-\omega \le -8t'$ and $4t+\omega < -8t'$, we first define

$$A \equiv \frac{2}{2\pi\sqrt{(4t+\omega-8t')(-8t'-4t+\omega)}} ,$$

$$q_2 \equiv \left[\frac{(-8t'-4t-\omega)(-8t'+4t-\omega)}{(-8t'+4t+\omega)(-8t'-4t+\omega)} \right]^{1/2} , \tag{C6a}$$

to write the final answer in the form,

$$I_4(\mathbf{q},\omega) = AF(\theta_3, q_2) ,$$

$$\theta_3 \equiv \begin{cases} \arcsin \left[\dfrac{-8t'+4t+\omega}{8t'+4t+\omega} \dfrac{8t'+\varepsilon_0}{\varepsilon_0-8t'} \right]^{1/2} & \text{if } 4t+\omega < \varepsilon_0 \le -8t' , \\ \pi/2 & \text{if } 4t-\omega < \varepsilon_0 \le 4t+\omega , \end{cases} \tag{C6b}$$

and

$$I_4(\mathbf{q},\omega) = A\left[F(\theta_2,q_2) + F\left[\frac{\pi}{2},q_2\right]\right],$$

$$\theta_2 \equiv \begin{cases} \arcsin\left[\dfrac{-8t'+4t+\omega}{-8t'+4t-\omega}\dfrac{4t-\omega-\varepsilon_0}{4t+\omega-\varepsilon_0}\right]^{1/2} & \text{if } 8t' < \varepsilon_0 \le 4t-\omega, \\ \pi/2 & \text{if } \varepsilon_0 < 8t'. \end{cases} \tag{C6c}$$

In the fourth and last region, where $4t-\omega > -8t'$, we have

$$I_4(\mathbf{q},\omega) = \frac{2}{2\pi\sqrt{(4t+\omega-8t')(-8t'+4t-\omega)}} F(\theta_4,q_3),$$

$$q_3 \equiv \left[\frac{-32\omega t'}{(4t+\omega+8t')(4t-\omega-8t')}\right]^{1/2},$$

$$\theta_4 \equiv \begin{cases} \arcsin\left[\dfrac{4t-\omega-8t'}{-16t'}\dfrac{-8t'-\varepsilon_0}{4t-\omega-\varepsilon_0}\right]^{1/2} & \text{if } 8t' < \varepsilon_0 < -8t', \\ \pi/2 & \text{if } \varepsilon_0 < 8t'. \end{cases} \tag{C7}$$

The answer is plotted in Fig. 23 for various chemical potentials. It is quite remarkable that a logarithmic divergence appears at $\omega = 4t + 8t'$ for all the fillings considered.

---

[1] M. S. Hybertsen, E. B. Stechel, W. M. C. Foulkes, and M. Schluter, Phys. Rev. B **45**, 10 032 (1992).

[2] W. E. Pickett, Rev. Mod. Phys. **61**, 433 (1989); M. S. Hybertsen, E. B. Setchel, M. Shluter, and D. R. Jennison, Phys. Rev. B **41**, 11 068 (1990).

[3] J. P. Lu, Q. Si, J. H. Kim, and K. Levin, Phys. Rev. Lett. **65**, 2466 (1990); Physica C **179**, 191 (1991); Q. Si, J. P. Lu, and K. Levin, Phys. Rev. B **45**, 4930 (1992); Q. Si, Y. Zhu, K. Levin, J. P. Lu, and J. H. Kim (unpublished).

[4] Y. Zha, Q. Si, and K. Levin (unpublished).

[5] H. Chi and A. D. S. Nagi, Phys. Rev. B **46**, 421 (1992).

[6] T. E. Mason, G. Aeppli, and H. A. Mook, Phys. Rev. Lett. **68**, 1414 (1992). Recently, the following relevant experimental work was pointed out to us: T. R. Thurston et al., Phys. Rev. B **46**, 9128 (1992); B. Keimer et al., ibid. **46**, 14 034 (1992).

[7] S. W. Cheong et al., Phys. Rev. Lett. **67**, 1791 (1991).

[8] R. J. Birgeneau et al., Phys. Rev. B **38**, 6614 (1988); T. R. Thurston et al., ibid. **40**, 4585 (1989); S. M. Hayden et al., Phys. Rev. Lett. **66**, 821 (1991); B. Keimer et al., Phys. Rev. Lett. **67**, 1930 (1991).

[9] J. M. Tranquada, in Proceedings of the University of Miami Workshop on Electronic Structure and Mechanisms for High T_c Superconductivity, edited by J. Ashkenazi and G. Vezzoli (Plenum, New York, 1991).

[10] (a) H. Chou et al., Phys. Rev. B **43**, 5554 (1991); P. Bourges et al., ibid. **43**, 8690 (1991); G. Shirane et al., Phys. Rev. Lett. **63**, 330 (1989); (b) J. M. Tranquada et al., Phys. Rev. B **46**, 5561 (1992). Note the similitude in shape between Fig. 7 of this paper and our Fig. 9. J. M. Tranquada et al., Phys. Rev. Lett. **64**, 421 (1992); B. J. Sternlieb, M. Sato, S. Shamoto, G. Shirane, and J. M. Tranquada, Phys. Rev. B **47**, 5320 (1993).

[11] J. Rossat-Mignot et al., Physica B **169**, 58 (1991); P. M. Gehring et al., Phys. Rev. B **44**, 2811 (1991).

[12] N. Bulut, D. Hone, D. J. Scalapino, and N. E. Bickers, Phys.

Rev. Lett. **65**, 2466 (1990); **64**, 2723 (1990); Phys. Rev. B **41**, 1797 (1990).

[13] N. Bulut and D. J. Scalapino, Phys. Rev. Lett. **68**, 706 (1992).

[14] A. J. Millis and H. Monien, Phys. Rev. B **45**, 3059 (1992).

[15] L. Chen, C. Bourbonnais, T. C. Li, and A.-M. S. Tremblay, Phys. Rev. Lett. **66**, 369 (1991).

[16] N. Bulut, Dynamics of Magnetic Fluctuations in High Temperature Superconductors, NATO Advanced Study Institute, edited by G. Reiter et al. (Plenum, New York, 1991); N. Bulut, D. J. Scalapino, and S. R. White, Phys. Rev. B **47**, 2742 (1993).

[17] N. Bulut and D. J. Scalapino (unpublished).

[18] J. Ruvalds, C. T. Rick, J. Zhang, and A. Virosztek, Science **256**, 1664 (1992).

[19] J. R. Schrieffer, X. G. Wen, and S. C. Zhang, Phys. Rev. B **39**, 11 663 (1989).

[20] J. Ruvalds and A. Virosztek, Phys. Rev. B **42**, 4064 (1990).

[21] H. J. Shulz, Phys. Rev. Lett. **64**, 1445 (1990).

[22] S. Wermbter and L. Tewordt, Phys. Rev. B **43**, 10 530 (1991); Physica C **196**, 383 (1992); **199**, 375 (1992).

[23] P. Bénard, Liang Chen, and A.-M. S. Tremblay, Phys. Rev. B **47**, 589 (1993).

[24] T. Moriya, Y. Takahashi, and K. Ueda, J. Phys. Soc. Jpn. **59**, 2905 (1990).

[25] D. R. Grempel and M. Lavagna, Solid State Commun. **83**, 595 (1992).

[26] T. Tanamoto, K. Kuboki, and H. Fukuyama, J. Phys. Soc. Jpn. **60**, 3072 (1991).

[27] H. Fukuyama, Prog. Theor. Phys. **108**, 287 (1992).

[28] R. R. P. Singh and R. L. Glenister, Phys. Rev. B **46**, 11 871 (1992).

[29] See Ref. 9 for a short review.

[30] P. B. Littlewood, J. Zaanen, G. Aeppli, and H. Monien (unpublished); P. B. Littlewood (unpublished).

[31] H. Monien (unpublished).

[32] C. M. Varma et al., Phys. Rev. Lett. **63**, 1996 (1989); **64**, 497

(1990); G. Kotliar, E. Abrahams, A. E. Ruckenstein, C. M. Varma, P. B. Littlewood, and S. Schmitt-Rink, Europhys. Lett. **15**, 655 (1991).

[33]H. Q. Lin and J. E. Hirsch, Phys. Rev. B **35**, 3359 (1987). These Monte Carlo simulations show the existence of antiferromagnetism when $t'\neq0$. Monte Carlo simulations also show an increase in the tendency to pairing when $t'\neq0$: R. R. dos Santos, Phys. Rev. B **39**, 7259 (1989); **46**, 5496 (1992).

[34]Daniel Groleau, M. Sc. thesis, Université de Sherbrooke, 1992, has found using crossing relations and Fermi-liquid theory that the effective mass is enhanced by a factor of at most 2 right at the incommensurate magnetic transition.

[35]This may not be true in the strong-coupling limit (see Ref. 28).

[36]J. H. Xu, T. J. Watson-Yang, Jaejun Yu, and A. J. Freeman, Phys. Lett. A **120**, 489 (1987).

[37]Note that in our approach we have neglected the effects of the superconducting phase transition on the incommensurate antiferromagnetic fluctuations since anyhow the experiments on which we concentrated (Fig. 1) are done in the normal state.

Detailed studies in the superconducting phase have appeared in Refs. 13 and in J. P. Lu, Phys. Rev. Lett. **68**, 125 (1992); as well as F. Marsiglio, Phys. Rev. B **47**, 5419 (1993).

[38]With incommensurate peaks, however, the ω/T scaling of nested Fermi liquids should not be recovered. This would be a test of nested Fermi-liquid theory (Ref. 20) since the position of the incommensurate peaks would fix the chemical potential which is usually taken as a fitting parameter in this approach.

[39]This was also noted in trying to explain NMR experiments (see Ref. 12).

[40]T. D. Mason (private communication).

[41]P. Montoux and D. Pines, Phys. Rev. Lett. **69**, 961 (1992).

[42]M. Gabay and M. T. Béal-Monod, Phys. Rev. B **18**, 5033 (1978). We thank A. Chubukov for pointing out this reference. See also, A. Isihara and T. Toyoda, Z. Phys. B **23**, 389 (1976).

[43]S. V. Maleyev, J. Phys. I France **2**, 181 (1992).